Published for SISSA by Springer

Received: November 20, 2017
Accepted: February 8, 2018
Published: February 19, 2018

Extra Higgs boson and Z' as portals to signatures of heavy neutrinos at the LHC

Elena Accomando,[a] **Luigi Delle Rose,**[a,b] **Stefano Moretti,**[a,b] **Emmanuel Olaiya**[b] **and Claire H. Shepherd-Themistocleous**[b]

[a] *School of Physics and Astronomy, University of Southampton, Highfield, Southampton SO17 1BJ, U.K.*

[b] *Particle Physics Department, Rutherford Appleton Laboratory, Chilton, Didcot, Oxon OX11 0QX, U.K.*

E-mail: E.Accomando@soton.ac.uk, L.Delle-Rose@soton.ac.uk, S.Moretti@soton.ac.uk, Emmanuel.Olaiya@stfc.ac.uk, Claire.Shepherd@stfc.ac.uk

Abstract: In this paper, we discuss the potential of observing heavy neutrino (ν_h) signatures of a $U(1)_{B-L}$ enlarged Standard Model (SM) encompassing three heavy Majorana neutrinos alongside the known light neutrino states at the Large Hadron Collider (LHC). We exploit the theoretical decay via a heavy (non-SM-like) Higgs boson and Z' production followed by $\nu_h \to l^{\pm}W^{\mp(*)}$ and $\nu_h \to \nu_l Z^{(*)}$ decays, ultimately yielding a $3l + 2j + E_T^{\rm miss}$ signature and, depending upon how boosted the final state objects are, we define different possible selections aimed at improving the signal to background ratio in LHC Run 2 data for a wide range of heavy neutrino masses.

Keywords: Beyond Standard Model, GUT, Higgs Physics, Neutrino Physics

ArXiv ePrint: 1708.03650

https://doi.org/10.1007/JHEP02(2018)109

JHEP02(2018)109

Contents

1 Introduction

Models with an additional Abelian group, U(1)$'$, with respect to the Standard Model (SM) symmetry can have their origin in a Grand Unification Theory (GUT) and it is possible for this extra symmetry to be broken at energies accessible at the CERN Large Hadron Collider (LHC). There are several realisations of GUTs that embed this dynamics, such as, e.g., E_6, String Theory motivated, SO(10) and Left-Right (LR) symmetric models [1–7].

An interesting phenomelogical case is where the conserved charge of the extra Abelian symmetry is $B - L$, with B and L the baryon and lepton numbers, respectively. This contains three heavy Right-Handed (RH) neutrinos, one extra heavy neutral gauge boson, Z', and an additional Higgs boson responsible for the U(1)$_{B-L}$ symmetry breaking. The cancellation of the U(1)$_{B-L}$ gauge and gravitational anomalies naturally predicts RH neutrinos that can be at the TeV scale, thus realising a low-scale seesaw mechanism for neutrino mass generation. Collider signatures emerging from such states are addressed in this paper.

While the signatures connected to the Z' and an additional Higgs boson have repeatedly been studied in the literature [7–21], the signatures emerging from the heavy neutrino sector have seen less investigation. From the diagonalisation of the neutrino mass matrix one obtains three very light, mostly Left-Handed (LH), neutrinos (ν_l), which are identified as the SM ones, and three heavy, mostly Right-Handed (RH), neutrinos (ν_h), with very small mixing with the light ν_l's, thereby obtaining very small yet non-vanishing couplings to the gauge bosons. Moreover, owing to the mixing in the scalar sector, the Yukawa interaction of the heavy neutrinos with the heavier Higgs, H_2, also provides the coupling of the ν_h's to the SM-like Higgs boson, H_1. These non-zero couplings enable, in particular, the $gg \to H_1 \to \nu_h\nu_h$ production mode if $m_{\nu_h} < m_{H_1}/2$ and the subsequent $\nu_h \to l^{\pm}W^{\mp *}$ and

JHEP02(2018)109

$\nu_h \to \nu_l Z^*$ (off-shell) decays [22, 23], an alternative to the case of SM-like Higgs decays instead into one light and one heavy neutrino [24–33].

A particular feature of such a heavy neutrino pair signature is that decay width of the heavy neutrino is small and its lifetime large, so that it turns out to be a long-lived particle and, over a large portion of the $\mathrm{U}(1)_{B-L}$ parameter space, its lifetime can be such that it can decay inside the LHC detectors, producing a distinctive Displaced Vertices (DVs) signature. This is due to the fact that the heavy neutrino couplings to the weak gauge bosons ($W^\pm$ and Z) are proportional to the ratio of light over heavy neutrino masses, which is extremely small in a type-I seesaw scenario. Ref. [34] showed the feasibility of establishing this signal at the LHC during Run 2, primarily because of a negligibly small background contribution.[1]

When the ν_h mass grows larger than $m_{H_1}/2$, the aforementioned production mode is no longer available, as the SM-like Higgs become immediately off-shell, owing to its small width, of 5 MeV or so. For $m_{H_1}/2 \lesssim m_{\nu_h} \lesssim M_{W,Z}$, DVs can be produced from heavy neutrinos in the heavy Higgs decays. For m_{ν_h} larger than the SM boson masses, simply because of the phase space enhancement entering the total width of the ν_h state, the latter stops producing DVs. Hence, one is forced to search for decay products which stem directly from the interaction point. In these conditions, the presence of the background becomes sizable. Furthermore, to stay with the aforementioned decay patterns, i.e., $\nu_h \to l^\pm W^\mp$ and $\nu_h \to \nu_l Z$, where the weak gauge bosons can be on-shell, one also realises that a significant boost can be given to the $W^\pm$ and Z decay products, so that they become more collimated in phase space as m_{ν_h} grows larger [35–37].

It is the purpose of this paper to examine heavy neutrino pair production and decay at the LHC, specifically for the signature $3l + 2j + E_T^{\mathrm{miss}}$ (where l represents an electron or muon, j a jet and E_T^{miss} the missing transverse energy), when their mass is the range $m_{\nu_h} > m_{H_1}/2$ up to the TeV scale. We shall see that two production mechanism will turn out to be useful, depending on the actual value of m_{ν_h}, namely, $gg \to H_2 \to \nu_h \nu_h$ (for intermediate mass values in the range $m_{H_1}/2 < m_{\nu_h} < m_{H_2}/2$) and $q\bar{q} \to Z' \to \nu_h \nu_h$ (for heavy mass values in the range $m_{H_2}/2 < m_{\nu_h} < M_{Z'}/2$). Notice in fact that the H_2 mass can be accessible at the LHC up to several hundreds of GeV while current limits on the Z' one are a few TeV [38–40].

This paper is organised as follows. Section 2 reviews the model under study together with an overview of its allowed parameter space. Then we describe the relevant production and decay processes of the heavy neutrino states in different sections depending on their mass, including presenting our numerical results. We then conclude in section 5.

2 A minimal Abelian extension of the SM

In this paper, we deal with a minimal renormalisable Abelian extension of the SM with only the matter content necessary to satisfy the cancellation of all gauge and gravitational anomalies. Hence, we augment each of the three lepton families by a RH neutrino which is

[1] An experimentally resolvable non-zero lifetime along with a mass determination for the heavy neutrino would potentially also enable an indirect measurement of the light neutrino mass, as remarked in ref. [9].

JHEP02(2018)109

a singlet under the SM gauge group with $B-L=-1$ charge. Furthermore, in the scalar sector, we introduce a complex scalar field χ, besides the SM-like Higgs doublet H, to trigger spontaneous symmetry breaking of the extra Abelian gauge group. The new scalar χ has $B-L=2$ charge and is a SM singlet. Its Vacuum Expectation Value (VEV), x, gives mass to the new heavy neutral gauge boson Z' and provides the Majorana mass to the RH neutrinos through a Yukawa coupling. (It is the latter that dynamically implements the type-I seesaw mechanism.)

The presence of two Abelian gauge groups allows for a gauge invariant kinetic mixing operator of the corresponding Abelian field strengths. This mixing is normally removed from the kinetic Lagrangian through a suitable transformation (rotation and rescaling), thus restoring its canonical form. However, it is reintroduced, through a coupling, $\tilde{g}$, in the gauge covariant derivative which thus acquires a non-diagonal structure

$$\mathcal{D}_\mu = \partial_\mu + \ldots + i g_1 Y B_\mu + i \left(\tilde{g} Y + g_1' Y_{B-L}\right) B'_\mu, \tag{2.1}$$

where Y and Y_{B-L} are the hypercharge and the $B-L$ quantum numbers, respectively, while B_μ and B'_μ are the corresponding Abelian fields. Other parameterisations, with a non-canonical diagonalised kinetic Lagrangian and a diagonal covariant derivative, are, however, completely equivalent. The details of the kinetic mixing and its relation to the $Z-Z'$ mixing, which we omit in this work, can be found in [9, 40, 41].

The $Z-Z'$ mixing angle in the neutral gauge sector is strongly bounded indirectly by the EW Precision Tests (EWPTs) and directly by the LHC data [40, 42–45] to small values, i.e, $|\theta'| \lesssim 10^{-3}$. In the $B-L$ model under study, we find

$$\theta' \simeq \tilde{g} \frac{M_Z\, v/2}{M_{Z'}^2 - M_Z^2}\,, \tag{2.2}$$

where v is the VEV of the SM-like Higgs doublet, H. In this case, the bound on the $Z-Z'$ mixing angle can be satisfied by either $\tilde{g} \ll 1$ or $M_Z/M_{Z'} \ll 1$, the latter allowing for a generous interval of allowed values for $\tilde{g}$.

After spontaneous symmetry breaking, two mass eigenstates, $H_{1,2}$, with masses $m_{H_{1,2}}$, are obtained from the orthogonal transformation of the neutral components of H and χ. The mixing angle of the two scalars is denoted by α. Moreover, we choose $m_{H_1} \leq m_{H_2}$ and we identify H_1 with the 125 GeV SM-like Higgs discovered at the LHC. The couplings between the light (heavy) scalar and the SM particles are equal to the SM rescaled by $\cos\alpha$ ($\sin\alpha$). The interaction of the light (heavy) scalar with the extra states introduced by the Abelian extension, namely the Z' and the heavy neutrinos, is controlled by the complementary angle $\sin\alpha$ ($\cos\alpha$).

Finally, the Yukawa Lagrangian is

$$\mathcal{L}_Y = \mathcal{L}_Y^{\rm SM} - Y_\nu^{ij}\, \overline{L^i}\, \tilde{H}\, \nu_R^j - Y_N^{ij}\, \overline{(\nu_R^i)^c}\, \nu_R^j\, \chi + \text{h.c.}, \tag{2.3}$$

where $\mathcal{L}_Y^{\rm SM}$ is the SM contribution. The Dirac mass, $m_D = 1/\sqrt{2}\, v Y_\nu$, and the Majorana mass for the RH neutrinos, $M = \sqrt{2}\, x Y_N$, are dynamically generated through the spontaneous symmetry breaking and, therefore, the type-I seesaw mechanism is automatically

JHEP02(2018)109

realised. Notice that M can always be taken to be real and diagonal without loss of generality. For $M \gg m_D$, the masses of the physical eigenstates, the light and the heavy neutrinos, are, respectively, given by $m_{\nu_l} \simeq -m_D M^{-1} m_D^T$ and $m_{\nu_h} \simeq M$. The light neutrinos are dominated by the LH SM components with a very small contamination of the RH neutrinos, while the heavier ones are mostly RH. The contribution of the RH components to the light states is proportional to the ratio of the Dirac and Majorana masses. After rotation into the mass eigenstates the charged and neutral currents interactions involving one heavy neutrino are given by

$$\mathcal{L} = \frac{g_2}{\sqrt{2}} V_{\alpha i}\, \bar{l}_\alpha \gamma^\mu P_L \nu_{h_i}\, W_\mu^- + \frac{g_Z}{2\cos\theta_W} V_{\alpha\beta} V_{\alpha i}^*\, \bar{\nu}_{h_i} \gamma^\mu P_L \nu_{l_\beta}\, Z_\mu \tag{2.4}$$

where $\alpha, \beta = 1, 2, 3$ for the light neutrino components and $i = 1, 2, 3$ for the heavy ones. The sum over repeated indices is implicit. In particular, $V_{\alpha\beta}$ corresponds to the Pontecorvo-Maki-Nakagawa-Sakata (PMNS) matrix while $V_{\alpha i}$ describes the suppressed mixing between light and heavy states. Notice also that the $Z\nu_h\nu_h$ vertex is $\sim V_{\alpha i}^2$ and, therefore, highly damped. These interactions are typical of a type-I seesaw extension of the SM. The existence of a scalar field generating the Majorana mass for RH neutrinos through a Yukawa coupling, which is a characteristic feature of the Abelian extensions of the SM, allows for the new and interesting possibility of producing a heavy neutrino pair from the SM-like Higgs (besides the obvious heavy Higgs mode). The corresponding interaction Lagrangian is given by

$$\mathcal{L} = -\frac{1}{\sqrt{2}} Y_N^k \sin\alpha\, H_1\, \bar{\nu}_{h_k} \nu_{h_k} = -g_1' \frac{m_{\nu_{h,k}}}{M_{Z'}} \sin\alpha\, H_1\, \bar{\nu}_{h_k} \nu_{h_k}, \tag{2.5}$$

where, in the last equation, we have taken the VEV to H_2 to be $x \simeq M_{Z'}/(2g_1')$. This expression neglects the sub-leading part that is proportional to $\tilde{g}$. For our purposes, this approximation can be safely adopted [13, 34]. The interaction between the light SM-like Higgs and the heavy neutrinos is not suppressed by the mixing angle $V_{\alpha i}$ but is controlled by the Yukawa coupling Y_N and scalar mixing angle α.

For illustrative purposes we assume that the PMNS matrix is equal to the identity matrix and that both neutrino masses, light and heavy, are degenerate in flavour. In this case the elements of the neutrino mixing matrix $V_{\alpha i}$ are simply given by $m_D/M \simeq \sqrt{m_{\nu_l}/m_{\nu_h}}$.

3 Heavy neutrino properties

Heavy neutrinos are characterised by a proper decay length that depends on the mass of the heavy neutrino itself and on the mass of the light neutrinos. This property has been discussed in detail in refs. [9, 34]. Here, we briefly summarise the result. In figure 1 (a), we plot the heavy neutrino's proper decay length as a function of the neutrino's mass for three different values of the light neutrino mass. The blue curve corresponds to the upper limit on the light neutrino mass. As one can see, the proper decay length decreases with increasing neutrino mass, ranging from 10^9 meters and more to lengths of the order of 10^{-5} meters. One can roughly define $m_{\nu h} \simeq M_W$ as a mass threshold for the heavy

JHEP02(2018)109

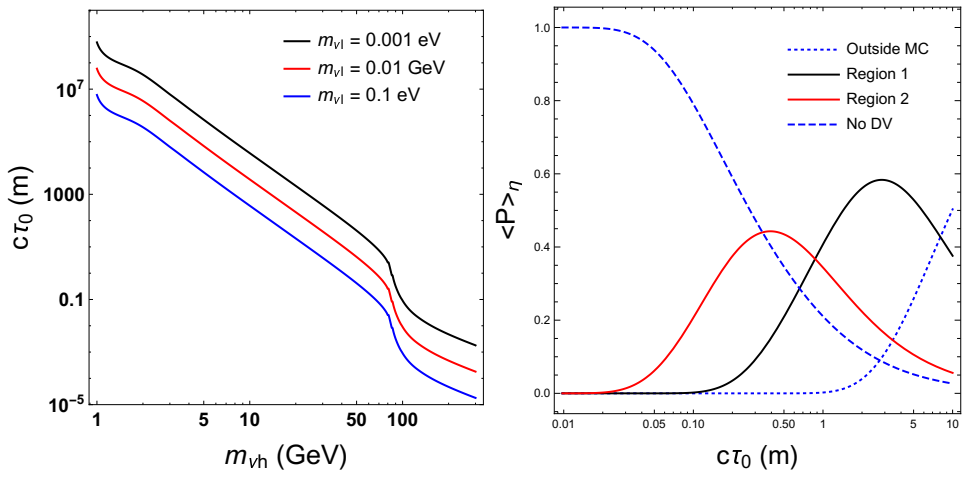

(a) (b)

Figure 1. (a) Proper decay length of the heavy neutrino as a function of the heavy neutrino mass m_{ν_h}. (b) Averaged decay probability of the heavy neutrino for $\beta\gamma = 1$ in different regions of the detector (see text).

neutrino that divides the short-lived from the long-lived regime. The difference between the two regimes is reflected in the detection strategy of such a particle. In figure 1 (b), we show the decay probability of the heavy neutrino in various regions of the detector defined below. The regions considered here do not cover all the detector and, therefore, the probabilities shown in figure 1 (b) do not sum up to 1. The probability is averaged over the pseudo-rapidity η of the heavy neutrino emitted off the parent particle, as a function of the proper decay length. The blue dashed line corresponds to the case when the heavy neutrino is detected like all other short-lived particles, i.e. no observable displaced vertices are produced. The red and black solid lines refer to the two cases when the heavy neutrino decays and generates a displaced vertex in the inner tracker and in the muon chamber, respectively. The dotted blue curve is when the neutrino decays outside the muon chamber, that is the heavy neutrino is undetected and gives rise to missing transverse energy. We refer to ref. [34] for the long-lived heavy neutrino search via displaced vertices techniques while in section 4, a study for detecting and reconstructing short-lived heavy neutrinos will be presented.

We summarise here the main production mechanisms of heavy neutrinos, giving an estimate of their expected cross section. The main mediators for heavy neutrino pair production are: the light SM-like Higgs, H_1, the heavy extra Higgs, H_2, and the heavy extra gauge boson Z'. The three contributing channels are:

- $gg \to H_1, H_2 \to \nu_h \nu_h$
- $q\bar{q} \to Z, Z' \to \nu_h \nu_h$

As all cross sections depend either directly or indirectly on the mass and the coupling of the Z'-boson, in figure 2 we display the 95% C.L. bounds on the gauge coupling g' and the mixing $\tilde{g}$ at fixed Z'-boson mass. We compute the 2σ significance contour at the 13 TeV

JHEP02(2018)109

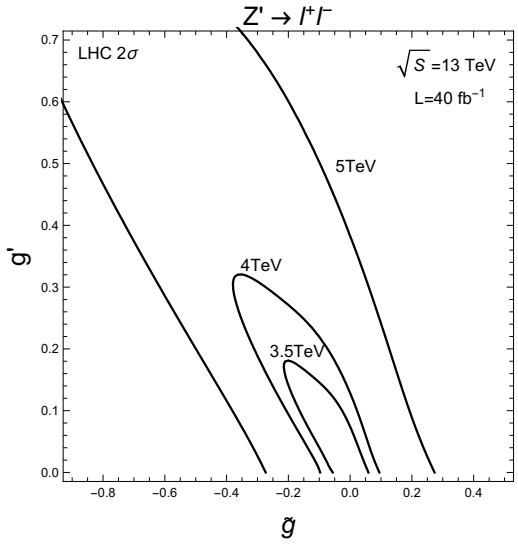

Figure 2. Significance analysis for the di-lepton ($l = e, \mu$) channel at the LHC for different Z' masses and $\mathcal{L} = 40\,\text{fb}^{-1}$.

LHC, using the acceptance times efficiency factor given by the CMS analysis [46] and assuming a total luminosity $\mathcal{L} = 40\,\text{fb}^{-1}$. We combine the electron and muon channels. In addition, as the Higgs mediated cross section depends on the scalar mixing angle, α, we take into account the exclusion limits on the α parameter as a function of the heavy Higgs mass and on the mass itself. Such limits have been enforced using `HiggsBounds` [47–51] and `HiggsSignals` [52] packages, see [40].

Given the allowed parameter space, we can compute the total cross sections for heavy neutrino production. In figure 3(a), we show the contour plots of the heavy neutrino pair production cross section via the light SM-like Higgs exchange in the plane (m_{ν_h}, α). We choose a value of the heavy Higgs VEV, $x = M_{Z'}/(2g') = 3.8\,\text{TeV}$, which is allowed according to figure 2. The cross section depends strongly on α, ranging from 1 to 300 fb with increasing α. In this case the heavy neutrinos must be lighter than 60 GeV to be produced on mass shell. They are thus predominantly long-lived particles and give rise to a signature characterised by displaced vertices. In figure 3(b), we display the analogous cross section mediated by the heavy Higgs, H_2. In this case, we assume $\alpha = 0.3$ and we plot the cross section contours in the plane (m_{ν_h}, m_{H_2}). The value of the cross section can range between 1 and 400 fb, as before. It is maximal for a relatively light H_2 with mass $m_{H_2} \leq 160\,\text{GeV}$ and consequently for relatively light neutrinos with $m_{\nu_h} \leq 75\,\text{GeV}$. Below this mass threshold, the H_2 branching fraction into heavy neutrinos is substantial while above this threshold the $H_2 \to W^+W^-$ channel opens up and becomes the dominant decay mode. For heavier neutrinos ($m_{\nu_h} \geq 75\,\text{GeV}$) one can still have a rather sizeable production cross section via H_2 exchange. For $m_{\nu_h} \geq M_W$, when the heavy neutrinos are predominantly short-lived particles, the cross section can be of the order of a few fb, depending on the heavy Higgs mass (see brown and green contours).

JHEP02(2018)109

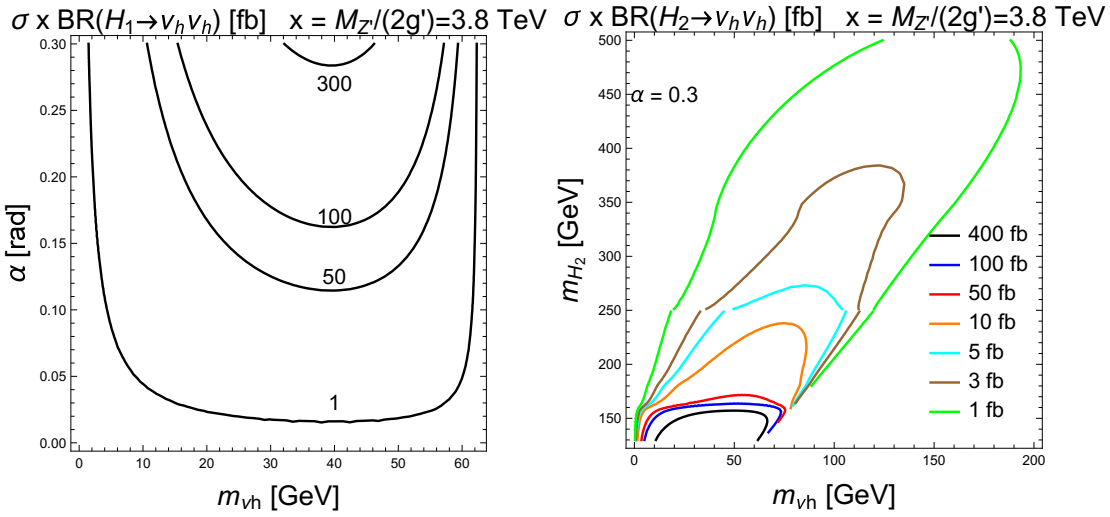

(a) (b)

Figure 3. (a) Contour plots of the cross section times BR for the process $pp \to H_1 \to \nu_h \nu_h$ at the LHC with $\sqrt{S} = 13\,\text{TeV}$ in the (m_{ν_h}, α) plane with $M_{Z'} = 5\,\text{TeV}$ and $g' \simeq 0.65$. (b) Contour plots of the cross section times BR for the process $pp \to H_2 \to \nu_h \nu_h$ at the LHC with $\sqrt{S} = 13\,\text{TeV}$ in the (m_{ν_h}, m_{H_2}) plane for $M_{Z'} = 5\,\text{TeV}$ and $g' \simeq 0.65$. The parameter x is the VEV of the extra scalar.

As H_1 and H_2 can contribute to the same final state for $m_{\nu_h} \leq 60\,\text{GeV}$, a priori they could interfere each other. We have therefore computed the gluon-induced total cross section $gg \to H_1, H_2 \to \nu_h \nu_h$ including the interference between the two contributions. In figure 4, we show the total heavy neutrino production cross section via scalars in the planes (m_{ν_h}, m_{H_2}) (see plot (a)) and (m_{ν_h}, α) (see plot (b)). We have explicitly checked that the interference is negligible . The total cross section reaches a maximum of about 700 fb with a light additional Higgs, $m_{H_2} \leq 150\,\text{GeV}$, and a maximal α value. For $m_{\nu_h} \geq 60\,\text{GeV}$, only H_2 contributes to the cross section whose value decreases with the heavy neutrino mass. For $m_{\nu_h} \geq 200\,\text{GeV}$, the cross section drops to fractions of a fb.

Finally, we consider the quark-antiquark induced channel mediated by the neutral gauge bosons, $q\bar{q} \to Z, Z' \to \nu_h \nu_h$. As the Z-boson contribution is small, we neglect it. In figure 5, we show the contour plots of the heavy neutrino production cross section via the Z'-boson exchange in the plane $(\tilde{g}, g')$ for two values of the Z' mass. The black contour with no label represents the 95% C.L. exclusion limit at fixed $M_{Z'}$ from figure 2. Compared to the cross section mediated by the scalars, the gauge mediated cross section is generally much smaller. In this case, one cannot exceed a fraction of a femtobarn, independently of the heavy neutrino mass. One can show that only in the high mass region of the neutrino spectrum, $m_{\nu_h} \gtrsim 200\,\text{GeV}$, this channel can in principle be competitive with the scalar mediated one and for $m_{\nu_h} \gtrsim 300\,\text{GeV}$ becomes the main production mode.

In summary, we can identify different regions of the heavy neutrino and heavy scalar spectra where different pair production mechanisms dominate. In the regime where heavy neutrinos are long-lived, namely $m_{\nu_h} < M_W$, we delineate the following categories:

JHEP02(2018)109

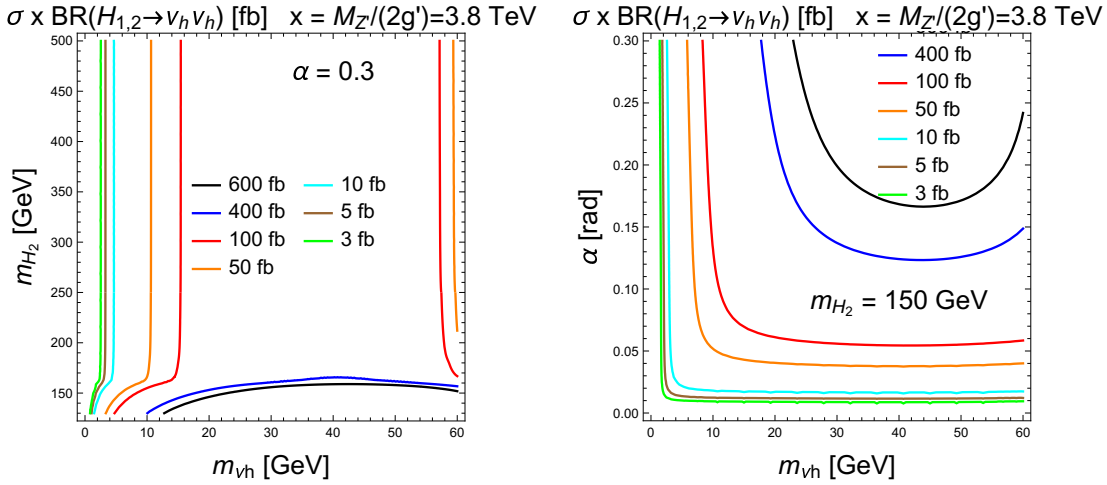

(a) (b)

Figure 4. (a) Contour plots of the cross section times BR for the process $pp \to H_{1,2} \to \nu_h \nu_h$ at the LHC with $\sqrt{S} = 13\,\text{TeV}$ in the (a) (m_{ν_h}, m_{H_2}) plane and (b) (m_{ν_h}, α) plane, with $M_{Z'} = 5\,\text{TeV}$ and $g' \simeq 0.65$. Notice that the cross sections for the channels induced by both H_1 and H_2 have been summed together. The interference is found to be negligible.

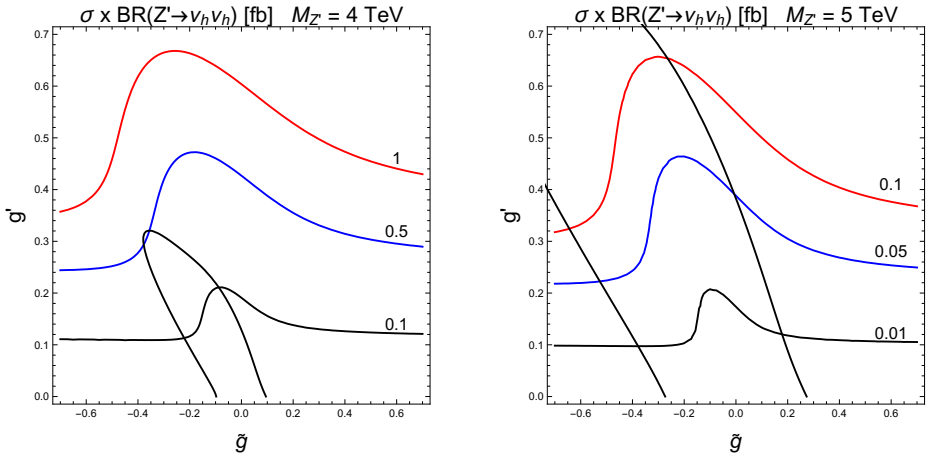

(a) (b)

Figure 5. Contour plots of the cross section times BR for the process $pp \to Z' \to \nu_h \nu_h$ at the LHC with $\sqrt{S} = 13\,\text{TeV}$ in the $(\tilde{g}, g')$ plane. The limit $m_{\nu_h} \ll M_{Z'}$ has been considered.

- $m_{\nu_h} < m_{H_1}/2$ and $m_{H_2} > 2m_W$

  The heavy neutrinos are relatively light, $m_{\nu h} \leq 60\,\text{GeV}$ and are produced from the decay of the SM-like Higgs. The heavier scalar predominantly decays into EW gauge bosons so that the heavy neutrino production cross section from H_2 is small compared to that of the corresponding SM-like Higgs mediated channel. In this low mass region of the spectrum, the heavy neutrinos are predominantly long-lived and give rise to displaced vertices in the detector. This case has been studied in [34].

JHEP02(2018)109

- $m_{\nu_h} > m_{H_1}/2$ and $2m_{\nu_h} < m_{H_2} < 2m_W$

  The heavy neutrinos are produced from the decay of the heavy Higgs with a sizeable cross section. For the maximal scalar mixing, $\alpha = 0.3$, the cross section can reach 400 fb. This region of the parameter space has been investigated in [34].

- $m_{\nu_h} < m_{H_1}/2$ and $2m_{\nu_h} < m_{H_2} < 2m_W$

  The two scalars H_1 and H_2 both contribute to the heavy neutrino pair production. The interference between the two contributions is negligible, thus in first approximation the two cross sections simply sum up giving rise to a sizeable total cross section that for the maximal scalar mixing, $\alpha = 0.3$ approaches 700 fb.

- The two scalars are almost decoupled, $\alpha \simeq 0$

  Both the heavy scalar production cross section and the heavy neutrino decay mode of H_2 are suppressed so that the heavy neutrinos cannot be produced through the scalars. The Z' production mode remains the only accessible channel despite its low cross section.

In the short-lived heavy neutrino scenario we identify two main regions:

- $m_{\nu_h} < m_{H_2}/2$ and $m_{\nu_h} \lesssim 300\,\text{GeV}$

  The heavy Higgs is the main production mode for the heavy neutrinos with a cross section of a few fb.

- $m_{\nu_h} > m_{H_2}/2$ or $m_{\nu_h} \gtrsim 300\,\text{GeV}$

  The heavy neutrino production from the H_2 is either kinematically forbidden or suppressed with respect to the Z' channel. Despite its small cross section, the Z' production mode through gauge interactions represents the main mechanism.

In ref. [34], we focused on the low to medium mass region of the heavy neutrino spectrum. There, the neutrino is very likely to be a long-lived particle giving rise to displaced vertices either in the inner tracker or in the muon chamber. The experimental techniques were described and the phenomenological analysis were carried out in ref. [34]. In this paper, we address the medium to high mass region of the neutrino spectrum where the particle is dominantly short-lived. In order to analyse this case, we choose a final state consisting of three leptons, two jets and missing transverse energy.

4 Short-lived heavy neutrinos: the $3l + 2j + E_T^{\text{miss}}$ signature

In the region of parameter space where the heavy neutrinos are short-lived, namely for masses $m_{\nu_h} \gtrsim M_W$ GeV, standard reconstruction techniques can be successfully employed. In this section we present a search for heavy neutrinos decaying into semi-leptonic final states, via $\nu_h \to l^{\mp}W^{\pm}$ and $\nu_h \to \nu_l Z$, characterised by three charged leptons (electrons and muons), two jets and missing energy at the LHC with a Centre-of-Mass energy of $\sqrt{S} = 13\,\text{TeV}$. The heavy neutrinos can be pair produced by the heavy Higgs state or by the

JHEP02(2018)109

Z' gauge boson, the latter being a characteristic property of abelian extensions of the SM. The study of this signal is particularly useful as it allows the reconstruction of both the mass of the heavy neutrinos and the mass of the mediator at the same time. Indeed, fully-leptonic final states would be characterised by a smaller cross section and more missing energy as a lepton pair originating from a heavy neutrino is always accompanied by a light neutrino as required by electric charge conservation. On the other hand, the final state with two leptons and four jets would suffer from a high SM background contamination. It is likely that if the mediator, either scalar or vector, is found at the LHC, it would first appear in other channels as DY for the Z' and $\gamma\gamma, ZZ, WW$ for the heavy Higgs. Therefore the reconstruction of its mass in its heavy neutrino decay mode would represent an independent measurement suggesting the existence of extra SM neutral states participating in the generation of the light neutrino masses.

The two production channels are characterised by distinctive kinematic features, indeed while the Z' mass limit is pushed beyond the 3 TeV region by searches in the di-lepton channel, the heavy Higgs mass is usually smaller than $\sim$ TeV to comply with the unitarity bounds. Therefore, if the heavy neutrino mass is below the TeV scale it is likely that it is highly boosted in the Z' case, thus giving rise to decay products poorly separated in the angular direction. Fat jet and jet substructure techniques can be employed to search for these particles.

The main sources of background are represented by the $WZjj$ associated production, $t\bar{t}l\nu$ production and $t\bar{t}$ pair production, the $WZjj$ representing the main contribution. In the first case the three leptons come from the $W^{\pm}$ and Z leptonic decays while in the $t\bar{t}l\nu$ case two jets and two leptons originate from the top-quark decay. In the last case the additional lepton is produced from the semi-leptonic decay of the B-meson. Notice that this lepton is not well isolated from the corresponding jet due to the large boost of the b quark. This feature can be successfully exploited to suppressed an otherwise overwhelming background.

We discuss separately the two signals in the following sections.

4.1 The heavy scalar mediator

We consider the three benchmark points in table 1 at a luminosity of $\mathcal{L} = 100\,\text{fb}^{-1}$. The other parameters are chosen to be $\alpha = 0.3$, $M_{Z'} = 5\,\text{TeV}$, $g' = 0.65$ and comply with the exclusion bounds from figure 2 and from Higgs searches. The simulation of signal and background has been performed with `CalcHEP` [53] at parton level using the U(1)$'$ model file [13, 14] accessible on the High Energy Physics Model Data-Base (HEPMDB) [54]. No resolution effect has been included and jets are identified with their partonic constituents. The event samples generated by `CalcHEP` are then rescaled by the corresponding cross sections and the given luminosity. For the first benchmark, BP1, the heavy neutrino pair production cross section is found to be $\sigma_{pp\to H_2\to\nu_h\nu_h} = 6.5\,\text{fb}$ where the heavy Higgs H_2 is produced through the gluon fusion process. With increasing m_{H_2}, the cross section decreses as displayed in table 1 for the benchmark BP2. The two heavy neutrinos predominantly decay into leptons and jets through the $W^{\pm}$ and Z gauge bosons by the following decay channels

JHEP02(2018)109

BP	m_{H_2} (GeV)	m_{ν_h} (GeV)	$\sigma(\nu_h\nu_h)$ (fb)
BP1	250	100	6.50
BP2	350	120	3.47
BP3	450	180	1.32

Table 1. Benchmark points for the heavy neutrino pair production via the heavy scalar. The first and second columns give the heavy Higgs and the heavy neutrino masses, respectively. The third column displays the total cross section.

- $\nu_h \to l^{\mp} W^{\pm} \to l^{\mp} l'^{\pm} \nu_{l'}$
- $\nu_h \to l^{\mp} W^{\pm} \to l^{\mp} \bar{q} q'$
- $\nu_h \to \nu_{l'} Z \to \nu_{l'} l^+ l^-$
- $\nu_h \to \nu_{l'} Z \to \nu_{l'} \bar{q} q'$
- $\nu_h \to \nu_{l'} Z \to \nu_{l'} \nu_l \nu_l$

where q can be one of the five light quarks and $l = e, \mu, \tau$ with τ decaying into e, μ and hadrons.

In order to perform our analysis, we first employ generic detector acceptance requirements to identify and reconstruct the three leptons and the two jets in the final state. As there are different trigger thresholds for different lepton flavour combinations, we need to divide the final state into four categories: 3μ, $2\mu e$, $2e\mu$, $3e$ ($+2j + E_T^{\rm miss}$). To reduce the turn on effect, we impose selection criteria a couple of GeV above the corresponding threshold. The transverse momentum criterion in each category is summarised below:

- $3\mu + 2j + E_T^{\rm miss}$: $p_{\mu_1}^T > 14\,\text{GeV}$, $p_{\mu_2}^T > 12\,\text{GeV}$, $p_{\mu_3}^T > 7\,\text{GeV}$
- $2\mu + e + 2j + E_T^{\rm miss}$: $p_l^T > 11\,\text{GeV}$
- $\mu + 2e + 2j + E_T^{\rm miss}$: $p_\mu^T > 10\,\text{GeV}$, $p_e^T > 14\,\text{GeV}$
- $3e + 2j + E_T^{\rm miss}$: $p_{e_{1,2}}^T > 28\,\text{GeV}$, $p_{e_3}^T > 5\,\text{GeV}$

In addition, we require that the pseudo-rapidity of each lepton satisfies $|\eta_l| < 2.5$. The two jets are characterised, instead, by $p_{j_{1,2}}^T > 30\,\text{GeV}$ and $|\eta_j| < 3$. To obtain isolated objects we require $\Delta R_{ll} > 0.3$ between any two leptons, $\Delta R_{jj} > 0.4$ for the two jets and $\Delta R_{lj} > 0.4$ between any lepton and jet. The corresponding efficiencies are shown in tables 2–5 for the two chosen benchmark points.

The smallest efficiency of the selection conditions of the signal events is related to the the p^T cuts due to the relative small mass of the heavy neutrinos that undergo a three-body decay into leptons and jets. For instance, in the BP1 case, the three-electron category is particularly affected by the trigger thresholds imposed, with an overall efficiency of the order of 6%. The three muon category has the best efficiency of about 30%, owing to the lowest asymmetric p^T cuts applied. Within all four categories, the decay objects

JHEP02(2018)109

are well isolated and therefore the angular separation cuts do not considerably affect the signal. The main contribution to the SM background comes from three processes: $WZjj$, $t\bar{t}$, and $t\bar{t}l\nu_l$. The SM background is initially dominant compared to the heavy neutrino pair production signal, as shown in tables 2–5, even after acceptance criteria (on η, p^T and Δ_R) which significantly reduce the background. In particular, the ΔR_{lj} criterion is quite effective in the suppression of the $t\bar{t}$ background as in this process the additional lepton coming from the B-meson decay is produced very close to the jet from which it originates. Yet, after the acceptance requirements (see entries in tables 2–5 above the horizontal line), the SM background is typically three orders of magnitude larger than the signal. The implementation of other kinematic cuts is thus needed to make the search for heavy neutrinos viable.

Since the two jets coming from the three-body decay of one of the two heavy neutrinos are always produced by the decay of a $W^{\pm}$-boson, one can require their invariant mass to be close to M_W, namely $|M_{jj} - M_W| < 20\,\text{GeV}$. This cut effectively reduces the background but it is not sufficient to distinguish the signal and the events from the $WZjj$ process still represent the main source of SM contamination. In order to improve the signal significance we require $|M_{l^+l^-} - M_Z| > 20\,\text{GeV}$ where $M_{l^+l^-}$ is the invariant mass of all the lepton pairs with opposite charge and same flavour, thus potentially identifying and removing the SM Z-gauge boson.

In order to visualise the strong impact of the reducible SM background and the effect of these kinematic cuts, in figure 6 (a) we show the distribution in the di-jet invariant mass. Here we sum up the number of events from all four categories, after the corresponding acceptance cuts defined above are applied. In figure 6 (b) we display the invariant mass of all the same-flavour and opposite-sign lepton pairs. This time, the additional cut $|M_{jj} - M_W| < 20\,\text{GeV}$ is superimposed on the acceptance constraints. The green line represents the $t\bar{t}l\nu$ while the red line is the $WZjj$ background. The blue line, the $t\bar{t}$ background, has been reduced to zero due to the $\Delta R_{lj} > 0.4$ requirement. After implementing the suggested kinematic cuts on the di-jet and di-lepton invariant masses, the SM background drops down by two orders of magnitude and more. This results in the background being roughly three times bigger than the signal for the 3μ-category when integrated over all masses (see tables 2–5).

In figure 7, we show two invariant mass distributions after the cuts discussed above. These observables can be used to extract the heavy Higgs mass. In particular, we show the transverse mass of all the visible particles M^T_{vis} and the invariant mass of all particles M_{all} including the light neutrino whose longitudinal momentum can be reconstructed through the W mass. Here, we sum up all events from the four above-mentioned categories. We then focus on the major aim of our paper that is reconstructing the heavy neutrino mass. From the shape of the M^T_{vis} distribution, one realises that a cut on this variable can help enhancing the signal over the SM background. We then impose that $|M^T_{\text{vis}} - m_{H_2}| < 50\,\text{GeV}$. With this constraint, the reducible SM background decreases by a factor of ten while the signal remains almost unaffected. The consequence is twofold. The significance increases by a factor of four, if one combines the four categories shown in tables 2–3, going from $S/\sqrt{B} = 1.4$ to $S/\sqrt{B} = 4.3$. In addition, using the invariant mass of the two jets and

JHEP02(2018)109

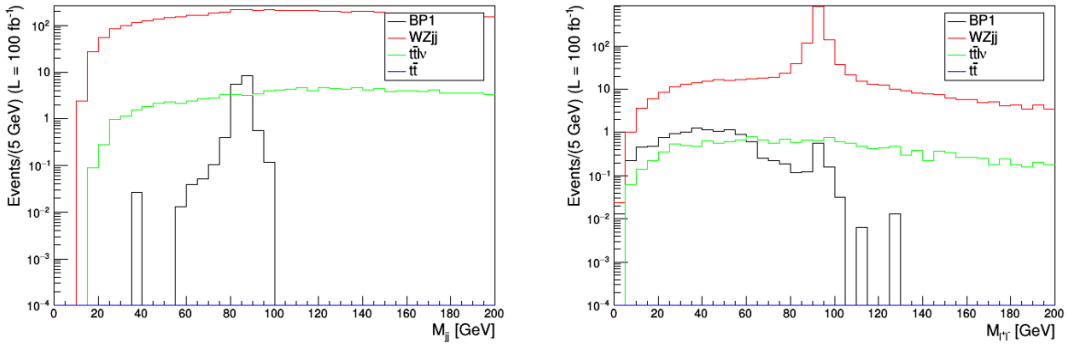

(a) (b)

Figure 6. (a) Distribution in the di-jet invariant mass for the benchmark point BP1. Acceptance cuts are applied. (b) Distribution in the di-lepton invariant mass for the benchmark point BP1. Acceptance cuts and $|M_{jj} - M_W| < 20\,\text{GeV}$ are applied. A luminosity $\mathcal{L} = 100\,\text{fb}^{-1}$ is assumed.

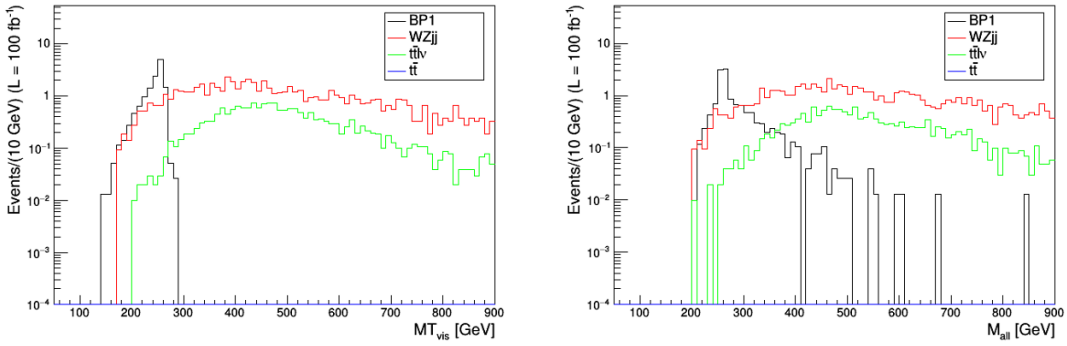

(a) (b)

Figure 7. (a) Distribution in the visible transverse mass of the final state. (b) Distribution in the total invariant mass of the final state obtained via a light neutrino reconstruction algorithm, as explained in the text. Acceptance cuts plus $|M_{jj} - M_W| < 20\,\text{GeV}$ and $|M_{l^+l^-} - M_Z| > 20\,\text{GeV}$ have been applied (see text). A luminosity $\mathcal{L} = 100\,\text{fb}^{-1}$ is assumed.

the closest lepton M_{ljj}, the reconstruction of the heavy neutrino mass is much clearer as shown in figure 8 where all four channels are combined. Analogous results are obtained when applying the cut $|M_{\text{all}} - m_{H_2}| < 50\,\text{GeV}$ with a final significance of $S/\sqrt{B} = 5.1$.

In the benchmark point BP2 of table 1, the heavy Higgs and the heavy neutrino masses increase. The neutrino pair production cross section goes down by roughly a factor of two, compared to the BP1 case, owing to the higher energy scale in the PDF's and to the opening of the $t\bar{t}$ decay channel for the heavy Higgs. In contrast, the trigger thresholds efficiency increases, because the heavy neutrino more massive. This feature is shown in tables 4–5. It is particularly striking for the *eee* category, characterised by the highest p^T cuts, where the efficiency raises from 6% (for BP1) to 30% (for BP2) just with a 20 GeV increase in the heavy neutrino mass. Altogether, the significance of the four combined channels is

JHEP02(2018)109

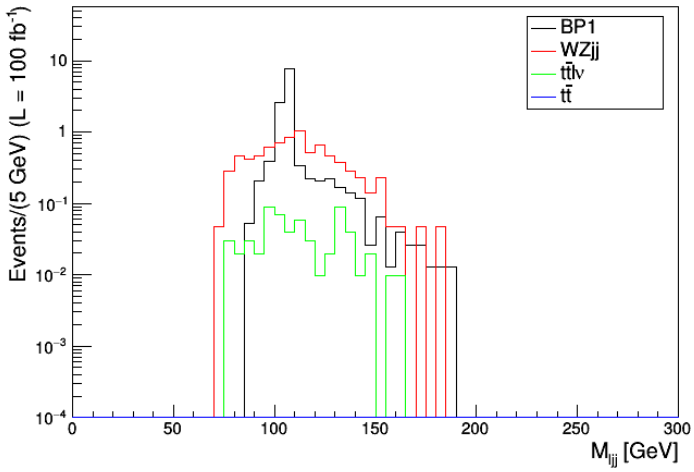

Figure 8. Distribution in the invariant mass of the two jets and the closest lepton, M_{ljj}, for the benchmark point BP1. Acceptance cuts plus $|M_{jj} - M_W| < 20\,\text{GeV}$, $|M_{l^+l^-} - M_Z| > 20\,\text{GeV}$ and $|M^T_{\text{vis}} - m_{H_2}| < 50\,\text{GeV}$ have been applied (see text). A luminosity $\mathcal{L} = 100\,\text{fb}^{-1}$ is assumed.

$S/\sqrt{B} = 1.5$ if the M^T_{vis} cut is used or $S/\sqrt{B} = 1.7$ if the M_{all} cut is employed instead, for a luminosity $\mathcal{L} = 100\,\text{fb}^{-1}$. If we increase the heavy Higgs and the heavy neutrino mass even further, the sensitivity goes down. In order to estimate the maximum $m_{\nu h}$ that one could explore in this channel, we have evaluated the BP3 reference point in table 1. Here we get three events at $\mathcal{L} = 100\,\text{fb}^{-1}$ and a significance $S/\sqrt{B} = 0.5$. Projecting to the High Luminosity Large Hadron Collider (HL-LHC) stage with $\mathcal{L} = 3\,\text{ab}^{-1}$, one reaches a significance $S/\sqrt{B} = 2.7$. The analysis in this channel is thus appropriate for the search of a heavy neutrino in the mass range $100\,\text{GeV} \leq m_{\nu h} \leq 180\,\text{GeV}$.

In the next section, we study the heavy neutrino pair production mediated by the heavy Z'-boson. This channel becomes complementary when the heavy neutrino is rather massive, $m_{\nu h} > 180\,\text{GeV}$, or in the decoupling limit when $\alpha = 0$.

4.2 The heavy Z' gauge boson mediator

In this section, we analyse the channel $pp \to Z' \to \nu_h \nu_h \to 3l + 2j + E_T^{\text{miss}}$. This process has been extensively studied in the past, see for example refs. [9], as it was considered the default production mechanism of heavy neutrinos. Owing to the present bounds on the mass of the extra heavy Z' boson, the cross section is now expected to be quite small. As shown in figure 5, $\sigma_{pp\to Z'\to\nu_h\nu_h} \leq 0.5\,\text{fb}$ for $M_{Z'} \geq 4\,\text{TeV}$.

The scope of our analysis is investigating new techniques in the attempt to enhance the heavy neutrino pair production signal over the background. As the Z' boson is quite massive, the produced heavy neutrinos are likely to be highly boosted for masses $m_{\nu_h} \leq 500\,\text{GeV}$. Their decay products will be boosted as well, giving rise to very collimated configurations in the final state. For higher masses $m_{\nu_h} \geq 500\,\text{GeV}$, the neutrinos wouldn't be boosted anymore but the two W-bosons coming from their decay would be. Therefore in either case, the two jets coming from the semi-leptonic decay of the neutrino, $\nu_h \to ljj$, will

JHEP02(2018)109

very likely be so close to each other so as to form a unique fat jet. This distinctive feature can be exploited in order to disentangle the signal from the overwhelming SM background. What differentiates the two cases of a relatively light and a quite heavy neutrino is the sub-structure of such a fat jet. When the heavy neutrino is relatively light and boosted, the fat jet will include inside its cone the lepton coming from the same three-body decay. If the neutrino is quite heavy, the lepton will remain well separated from the fat jet.

In order to depict the two highlighted situations, we choose the following set of parameters allowed by present direct and indirect searches: $M_{Z'} = 4\,\text{TeV}$, $g' = 0.3$ and $\tilde{g} = -0.3$ with a decoupled heavy Higgs. We consider the two benchmark points characterised by different heavy neutrino masses: BP1 with $m_{\nu_h} = 400\,\text{GeV}$ ($\sigma(pp \to Z' \to \nu_h \nu_h = 0.37\,\text{fb}$) and BP2 with $m_{\nu_h} = 1000\,\text{GeV}$ ($\sigma(pp \to Z' \to \nu_h \nu_h = 0.26\,\text{fb}$).

To start with, we analyse the kinematics of the produced $3l + 2j + E_T^{\text{miss}}$ events. We firstly examine the BP1 scenario, characterised by the production of a pair of boosted heavy neutrinos. In figure 9, we show the transverse momentum distribution of the leading lepton (plot a), the sub-leading lepton (plot b), the third least energetic lepton (plot c) and of the two jets (plot d). In estimating the signal and background efficiencies, unlike the previous H_2-mediated process, we show the sum of the events over the four lepton categories. Indeed, there is not much difference in the efficiency between the four signal types, $ee\mu$, $e\mu\mu$ and $\mu\mu\mu$, owing to the much larger heavy neutrino mass. Altogether, the basic selection cuts have an average efficiency of about 75%. In order to suppress the SM background, we impose more stringent cuts on the transverse momentum of the leptons. Based on the observation of plots (a)–(c) of figure 9, the following constraints have been chosen:

- $p_{l_1}^T > 300\,\text{GeV}$, $p_{l_2}^T > 150\,\text{GeV}$, $p_{l_3}^T > 15\,\text{GeV}$

The efficiency of the signal remains 64% while the background sources are heavily suppressed, with an efficiency of less than 1%. In figure 9, we show the distribution in ΔR_{lj} (plot e), averaged over the six possible lepton-jet pairs, and ΔR_{jj} (plot f). Clearly, while any leptons and jets are well separated from each other (same is true for the separation between any two leptons), the two jets coming from the W-boson decay are typically collimated. Requiring the two jets and the three leptons to be resolved separately via $\Delta R_{jj,lj} > 0.4$ and $\Delta R_{ll} > 0.3$ takes the signal efficiency down to roughly 20%. Globally, these selection cuts reduce the signal by a factor of seven but they help decrease the SM background substantially, which goes down by almost three orders of magnitude. Notice that the separation lepton-jet suppresses completely the $t\bar{t}$ source of background. The additional cut $\Delta R_{jj} < 1.5$ further reduces the $WZjj$ and $t\bar{t}l\nu$ background components by two thirds. Finally, two cuts on the same-flavour opposite-sign di-lepton and di-jet invariant masses are imposed. The global efficiencies are shown in table 6. Despite of all these cuts, the SM background is still of the same order as the signal. Looking at the total visible mass distribution of the final state, one realises that signal and background occupy the same regions. The cut $|M_{\text{vis}}^T - M_{Z'}| \leq 1\,\text{TeV}$ reduces the SM background to zero, affecting the signal only marginally. We obtain an analogous result if we impose $|M_{\text{all}} - M_{Z'}| \leq 1\,\text{TeV}$ via the light neutrino reconstruction algorithm. Despite the success

JHEP02(2018)109

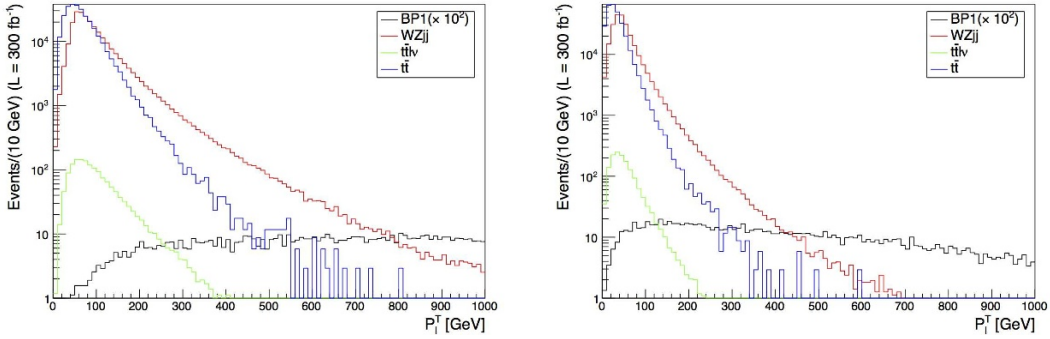

(a) most energetic lepton p^T

(b) second most energetic lepton p^T

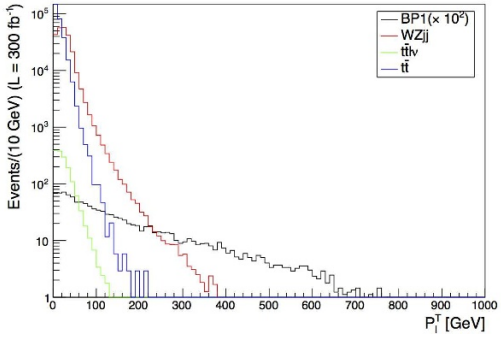

(c) least energetic lepton p^T

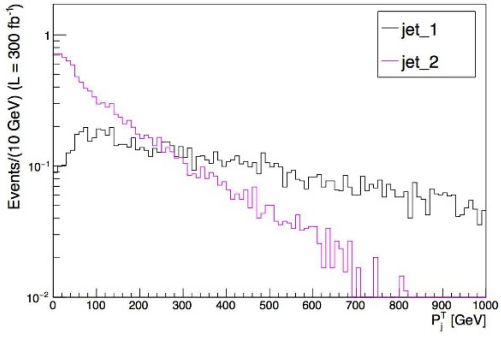

(d) leading and sub leading jet p^T

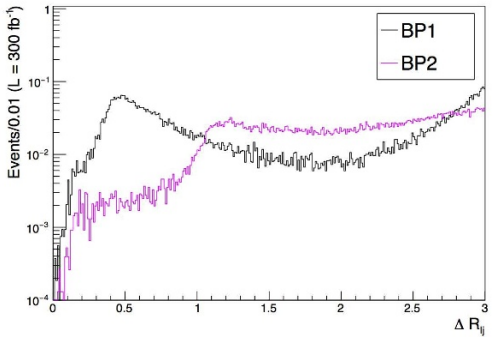

(e) lepton-jet angular separation ΔR_{lj}

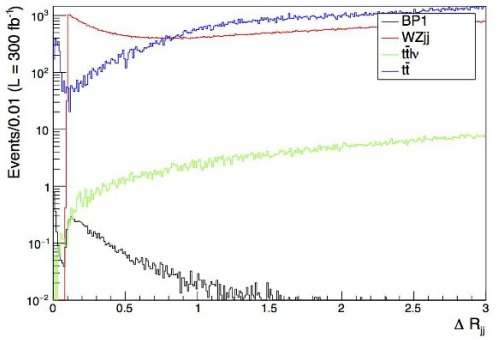

(f) jet angular separation ΔR_{jj}

Figure 9. (a) Distribution in the transverse momentum of the leading lepton. The black solid line is the signal, the red line the $WZjj$ background, the green and the blue lines the $t\bar{t}l\nu$ and $t\bar{t}$ SM background components. (b) same as (a) for the second most energetic lepton. (c) same as (a) for the least energetic lepton. (d) Distribution in the transverse momentum of the two jets in BP1. Black and magenta lines refer to the leading and sub-leading jet, respectively. (e) Distribution in the angular separation between any jet and lepton averaged over the six possible pairs. The black and magenta lines refer to BP1 and BP2, respectively. (f) Distribution in the angular separation between the two jets. The color code is the same as for plot (a). All distributions are calculated for the benchmark point BP1 (except plot (e)) for a luminosity $\mathcal{L} = 300\,\text{fb}^{-1}$.

JHEP02(2018)109

of suppressing the huge SM background, the number of signal events left is very small (one in this specific case).

Similar conclusions hold for the benchmark point BP2 where $m_{\nu h} = 1\,\text{TeV}$. The distinctive characteristic compared to the previous case is the angular separation of the leptons from the jets. As one can see in figure 9 (e), the ΔR_{lj} is shifted towards higher values. Therefore, the corresponding signal efficiencies increase. As a result, despite the lower initial cross section, the number of events after the cut flow is roughly the same as shown in table 6. So our conclusion is that this analysis, carried out with standard techniques, requires very high luminosity and is thus tailored for the HL-LHC. In the next section, we explore an advanced experimental strategy based on the so called fat jet. This attempt relies on the observation that the two produced jets are quite collimated, giving rise to a unique large hadronic cone, owing either to the boosted heavy neutrino (BP1) or to the boosted W-boson coming from the heavy neutrino decay (BP2).

4.2.1 Fat jet technique

In this section, we exploit fat jets, where a fat jet is a parton with a ΔR radius of 0.8, to see whether the significance of the Z'-mediated production of heavy neutrinos can be increased. With respect to the previous case, where the two jets are isolated and separately reconstructed, one is forced to introduce WZj in the simulation as another source of background.

The fat jet is defined by the following two categories:

- one single leading jet with $p_{j_1}^T > 200\,\text{GeV}$
- two jets with separation $\Delta R_{jj} \leq 0.8$ and global transverse momentum $p_J^T \geq 200\,\text{GeV}$, with $J = j_1 + j_2$.

As displayed in table 7, the fat jet selection criterion defined above has an efficiency on the signal of more than 79%, depending on the transverse momentum threshold and the mass of the heavy neutrino. This is a significant improvement as the default di-jet selection, which we discussed previously, has only an efficiency of less than 20% for the signal. The choice of the P^T threshold for identifying the fat jet is not really significant for the signal. In the range $100\,\text{GeV} \leq p_J^T \leq 200\,\text{GeV}$, no dramatic variation is observed in the selection efficiency as shown in table 7. Where it really helps is in reducing the SM background. For that reason, we choose the value $p_J^T > 200\,\text{GeV}$. We also impose that all the sub-leading jets, if present, have $p_j^T < 0.25\,p_J^T$. This restriction has the advantage to clean the signal (in which case the two jets are merged into a single fat jet) removing any other jet activity originating from initial state radiation, pile-up or τ hadronic decays. It also suppresses the backgrounds (with the only exception of WZj) as the two jets are expected to be well isolated from each other. Therefore, requiring a hierarchy between the leading fat jet and the sub leading one will reject all the events for which the two jets are characterised by the same p^T.

For the leptons, besides the standard geometric acceptance requirement $|\eta_l| < 2.5$, we apply the set of cuts on the transverse momentum as before: $p_{l_1}^T > 300\,\text{GeV}$, $p_{l_2}^T > 150\,\text{GeV}$

JHEP02(2018)109

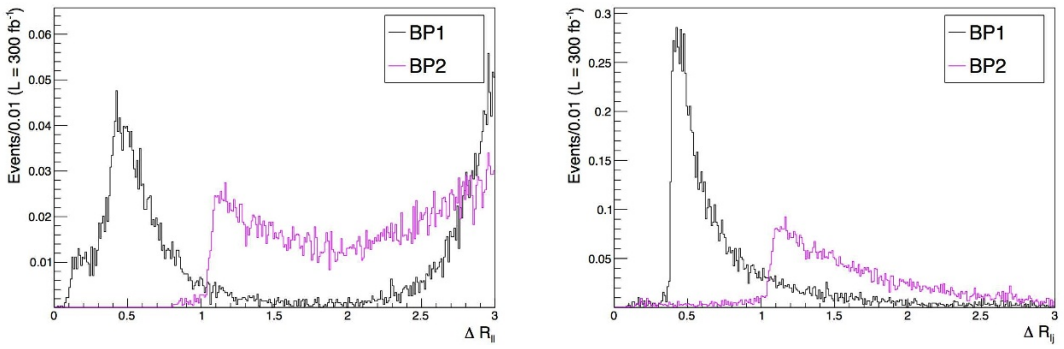

(a) (b)

Figure 10. (a) Distribution in the angular separation between the leptons averaged over the three possible pairs. Black and magenta lines refer to BP1 and BP2 scenarios, respectively. (b) Distribution in the angular separation between the fat jet and the closest lepton. The color code is the same as in (a). A luminosity $\mathcal{L} = 300\,\text{fb}^{-1}$ is assumed.

and $p_{l_3}^T > 15\,\text{GeV}$. This selection is particularly effective in suppressing the background to a few percent of its initial value. The selections described above are common to both the two BPs and rely only on the boosted topology and on the very energetic nature of the final state objects, which is a direct consequence of the large Z' mass.

For the BP1 we furthermore require that one lepton lies inside the fat jet, while the other two leptons are well separated from each other via $\Delta R_{ll} > 0.3$ and outside the fat jet cone, $\Delta R_{lJ} > 0.8$. This choice is motivated by the kinematic features of the BP, described in the previous section, and supported by the analysis of the angular separation between these particles.

In figure 10, we plot the distribution in the separation variable between two leptons ΔR_{ll}, averaged over all lepton pairs, (plot a) and between the fat jet and its closest lepton ΔR_{lJ} (plot b). From there, it is evident that one of the leptons is very close to this fat jet. If we require that the three leptons are all well separated from the fat jet, $\Delta R_{lJ} > 0.8$, the number of signal events drops by a factor of five. The most probable configuration is when the lepton is inside the fat. When we require only two leptons to be separated from the fat jet, the efficiency in fact increases up to about 82% as shown in the sixth row of table 7.

In principle, the lepton that may fall inside the fat jet can be disentangled from the jet and individually reconstructed. An additional cut that is particularly effective in suppressing the background while leaving the signal almost unaffected consists of imposing a lower value on the transverse momentum of the lepton with respect to the direction of the jet [55]. In particular, this cut removes the SM $t\bar{t}$ background and compensates for the absence of the isolation requirement on the lepton inside the fat jet which was very effective in the standard analysis in the removal of events with a lepton emerging from the B meson decay.

JHEP02(2018)109

Finally, the cut on the invariant mass of lepton pairs is imposed as described in the previous analyses in order to reject events from the $WZjj$ and WZj backgrounds where two same flavour and opposite sign leptons are generated from the Z decay.

The full cut flow is shown in table 8 for the two benchmark points BP1 and BP2. After the full cut flow, the SM background is zero. The number of signal events is around four at $\mathcal{L} = 300\,\text{fb}^{-1}$. Even though this means a small number of events given the projected luminosity of Run II, such a number can become significant at the HL-LHC stage, as the signal is almost background free.

Analogous results are obtained for the benchmark point BP2. This scenario, characterised by a very heavy neutrino $m_{\nu h} = 1000\,\text{GeV}$, differs from the previous one in the angular separation between leptons and fat jet. In this case all the leptons are well separated from the fat jet ($\Delta R_{lJ} > 0.8$) as clear from figure 10(a). We therefore do not require the presence of any lepton inside the fat jet. The remaining cut flow is identical to the BP1 scenario and at the end the number of signal events is same, i.e. four at $\mathcal{L} = 300\,\text{fb}^{-1}$. These events are also almost background free as shown in table 8.

The fat jet analysis appears to be more competitive than the standard technique in searching for these low signal yields. For the discussed characteristics, this seems to be an ideal study for the HL-LHC option [56], which goes beyond this particular Z'-boson analysis.

5 Conclusions

The experimental evidence of neutrino flavour oscillations, implying that such states of Nature have a mass, is a pressing problem for the SM. An economical solution to account for these is to extend the SM gauge group by an additional Abelian $\text{U}(1)_{B-L}$ symmetry, broken through a Higgs mechanism, thereby yielding simultaneously new Higgs (H_2) and gauge (Z') bosons, one of each, acting as heavier companions to the SM(-like) H_1 and Z states. As a byproduct of this dynamics, one then gets three additional heavy neutrinos, of a Majorana nature, following the customary requirement of avoiding gauge and gravitational anomalies. Then, a Type-I seesaw is responsible for neutrino mass generation and mixing, leaving behind the three SM-like light neutrinos (ν_l) and three heavy (ν_h) ones, which can then be at the EW or TeV scale. Since the limits on additional Higgs and gauge bosons of the kind we introduced here are presently set in the same energy ranges, respectively, one is tempted to access all the additional states of this theoretical construct at once, by pursuing the search for pair production of heavy neutrino states emerging from the decay of H_2 and Z' bosons, so that the latter act as portals to the former.

The parameter space of this scenario, tested against all available theoretical and experimental constraints, was already defined in a previous publication [40] (see also [38, 39]), where potential feasibility of the aforementioned production and decay modes was highlighted, based on inclusive analyses. In this paper, which follows closely ref. [34], where the $gg \to H_{1,2} \to \nu_h\nu_h$ signal was proved to be accessible during Run 2 of the LHC in essentially a background free environment by exploiting DVs induced by rather light ν_h states yielding signatures with two to four leptons, we assessed the possibility of accessing heavier

JHEP02(2018)109

ν_h states, by exploiting $gg \to H_2 \to \nu_h\nu_h$ and $q\bar{q} \to Z' \to \nu_h\nu_h$ signals, for which DVs are no longer available. The analysis in these conditions is much more challenging, as the heavy neutrino decay products stem from the interaction point, where the SM background is initially overwhelming.

However, upon a dedicated analysis of the $3l + 2j + E_T^{\rm miss}$ signature emerging from both production and decay modes (i.e., via H_2 and Z' intermediate states), we have been able to prove that some evidence of the existence of ν_h states can already be glimpsed with standard luminosity conditions ($\mathcal{L} = 100\,{\rm fb}^{-1}$) during the 13 TeV runs of the LHC, though full discovery will probably have to wait for the high luminosity option of the machine, the so-called High Luminosity LHC (HL-LHC) [56]. We have come to this encouraging conclusion after adopting a rather sophisticated signal-to-background selection. In doing so, we had to devise different approaches depending on the relative mass differences amongst the Z', H_2 and ν_h states (as well as $W^\pm$ and Z bosons, which appear in the two ν_h decay chains), since — depending on these — one may have more or less boosted objects in the detector, thus ranging from the case of all reconstructed particles being separated to the one where the two jets could be merged by standard jet clsutering algorithms into a single fat one (for which then we had to exploit jet substructure techniques) with and without a lepton inside it. To facilitate our studies, we have made use of a variety of triggers available for current and subsequent runs of the LHC collider.

As emphasised in refs. [38–40], simultaneous access to the $gg \to H_1 \to \nu_h\nu_h$, $gg \to H_2 \to \nu_h\nu_h$ and $q\bar{q} \to Z' \to \nu_h\nu_h$ modes would finally enable one to establish a direct link between measurements obtainable at the EW scale and the dynamics of the underlying model up to those where a GUT scenario embedding a $\mathrm{U}(1)_{B-L}$ can be realised. In short, with the present paper, we have completed the analysis of the $\mathrm{U}(1)_{B-L}$ signatures that need establishing at the LHC in order to pursue such an endeavour. In future publications, we shall see their deployment in fully fledged experimental analyses.

Acknowledgments

EA, LDR, SM and CHS-T are supported in part through the NExT Institute. The work of LDR has been supported by the STFC/COFUND Rutherford International Fellowship scheme.

JHEP02(2018)109

	BP1(eee)	Eff. %	$WZjj$	Eff. %	$t\bar{t}l\nu$	Eff. %	$t\bar{t}$	Eff. %	$S/\sqrt{B}$
No cuts.	36.3692	100	18271.1	100	60.0229	100	7064.84	100	0.228219
η	26.7929	73.67	9292.88	50.86	42.1034	70.15	5383.75	76.2	0.220844
p^T	1.74115	6.499	3646.03	39.23	25.8532	61.4	1194.66	22.19	0.0249589
ΔR	1.4293	82.09	3174.62	87.07	21.8961	84.69	0	0	0.0252805
$\lvert M_{jj} - M_W\rvert < 20\,\text{GeV}$	1.4293	100	379.156	11.94	3.19114	14.57	0	100	0.0730963
$\lvert M_{l^+l^-} - M_Z\rvert > 20\,\text{GeV}$	1.0135	70.91	11.0076	2.903	1.80668	56.62	0	100	0.283125
$\lvert M^T_{\text{vis}} - m_{H_2}\rvert < 50\,\text{GeV}$	1.00051	98.72	0.60635	5.508	0.0490945	2.717	0	100	1.23582
$\lvert M_{\text{all}} - m_{H_2}\rvert < 50\,\text{GeV}$	0.844587	83.33	0.233212	2.119	0.0098189	0.5435	0	100	1.71322

	BP1($ee\mu$)	Eff. %	$WZjj$	Eff. %	$t\bar{t}l\nu$	Eff. %	$t\bar{t}$	Eff. %	$S/\sqrt{B}$
No cuts.	38.89	100	19574.3	100	185.155	100	21486.4	100	0.191491
η	28.625	73.61	9957.39	50.87	130.277	70.36	16520.9	76.89	0.175483
p^T	3.70319	12.94	3652.42	36.68	76.7151	58.89	3164.68	19.16	0.0446012
ΔR	3.14446	84.91	3177.7	87	65.0109	84.74	0	0	0.0552195
$\lvert M_{jj} - M_W\rvert < 20\,\text{GeV}$	3.13147	99.59	377.85	11.89	8.31661	12.79	0	100	0.159353
$\lvert M_{l^+l^-} - M_Z\rvert > 20\,\text{GeV}$	2.80663	89.63	21.3155	5.641	6.79468	81.7	0	100	0.529362
$\lvert M^T_{\text{vis}} - m_{H_2}\rvert < 50\,\text{GeV}$	2.70268	96.3	2.70526	12.69	0.147283	2.168	0	100	1.60022
$\lvert M_{\text{all}} - m_{H_2}\rvert < 50\,\text{GeV}$	2.2479	80.09	1.35263	6.346	0.0589134	0.8671	0	100	1.89204

Table 2. Benchmark point BP1. Luminosity $\mathcal{L} = 100\,\text{fb}^{-1}$. Universal acceptance cuts = $|\eta_l| < 2.5$, $|\eta_j| < 3$, $p^T_{j1,2} > 30\,\text{GeV}$, $\Delta R_{jj} > 0.4 + \Delta R_{lj} > 0.4 + \Delta R_{ll} > 0.3$. Transverse momentum cuts for the eee category: $p^T_{e_{1,2}} > 28\,\text{GeV}$ and $p^T_{e_3} > 5\,\text{GeV}$. Transverse momentum cuts for the $ee\mu$ category: $p^T_{e_{1,2}} > 14\,\text{GeV}$ and $p^T_{\mu} > 10\,\text{GeV}$. Notice that here and in all the following tables, 0 events means the estimated value is less than 10^{-4}.

	BP1($e\mu\mu$)	Eff. %	$WZjj$	Eff. %	$t\bar{t}l\nu$	Eff. %	$t\bar{t}$	Eff. %	$S/\sqrt{B}$
No cuts.	38.0454	100	19613.8	100	187.639	100	21109.9	100	0.188096
η	27.7155	72.85	10031.1	51.14	132.82	70.78	16298.2	77.21	0.170377
p^T	5.17147	18.66	3776.77	37.65	81.6147	61.45	3599.54	22.09	0.0598832
ΔR	4.08001	78.89	3287.72	87.05	69.8418	85.58	0	0	0.0704123
$\lvert M_{jj} - M_W\rvert < 20\,\text{GeV}$	4.05402	99.36	394.687	12	9.82872	14.07	0	100	0.201566
$\lvert M_{l^+l^-} - M_Z\rvert > 20\,\text{GeV}$	3.91109	96.47	25.6999	6.511	8.02204	81.62	0	100	0.673506
$\lvert M^T_{\text{vis}} - m_{H_2}\rvert < 50\,\text{GeV}$	3.70319	94.68	2.70526	10.53	0.314205	3.917	0	100	2.13114
$\lvert M_{\text{all}} - m_{H_2}\rvert < 50\,\text{GeV}$	2.92357	74.75	1.25934	4.9	0.117827	1.469	0	100	2.49127

	BP1($\mu\mu\mu$)	Eff. %	$WZjj$	Eff. %	$t\bar{t}l\nu$	Eff. %	$t\bar{t}$	Eff. %	$S/\sqrt{B}$
No cuts.	35.6546	100	18102	100	64.9422	100	6901.4	100	0.225192
η	26.4941	74.31	9214.47	50.9	45.9328	70.73	5336.08	77.32	0.219293
p^T	7.74422	29.23	3910.77	42.44	32.4907	70.74	1428.14	26.76	0.105666
ΔR	6.5488	84.56	3401.86	86.99	27.7482	85.4	0	0	0.111825
$\lvert M_{jj} - M_W\rvert < 20\,\text{GeV}$	6.5488	100	413.624	12.16	3.85883	13.91	0	100	0.320511
$\lvert M_{l^+l^-} - M_Z\rvert > 20\,\text{GeV}$	5.43135	82.94	15.252	3.687	2.16016	55.98	0	100	1.30161
$\lvert M^T_{\text{vis}} - m_{H_2}\rvert < 50\,\text{GeV}$	5.13249	94.5	1.91234	12.54	0.0785512	3.636	0	100	3.63752
$\lvert M_{\text{all}} - m_{H_2}\rvert < 50\,\text{GeV}$	3.96306	72.97	0.746277	4.893	0.0392756	1.818	0	100	4.4714

Table 3. Benchmark point BP1. Luminosity $\mathcal{L} = 100\,\text{fb}^{-1}$. Universal acceptance cuts = $|\eta_l| < 2.5$, $|\eta_j| < 3$, $p^T_{j_{1,2}} > 30\,\text{GeV}$, $\Delta R_{jj} > 0.4 + \Delta R_{lj} > 0.4 + \Delta R_{ll} > 0.3$. Transverse momentum cuts for the $e\mu\mu$ category: $p^T_{l_{1,2,3}} > 11\,\text{GeV}$ ($l = e, \mu$). Transverse momentum cuts for the $\mu\mu\mu$ category: $p^T_{\mu_1} > 14\,\text{GeV}$, $p^T_{\mu_2} > 12\,\text{GeV}$ and $p^T_{\mu_3} > 7\,\text{GeV}$.

	BP2(eee)	Eff. %	$WZjj$	Eff. %	$t\bar{t}l\nu$	Eff. %	$t\bar{t}$	Eff. %	$S/\sqrt{B}$
No cuts.	13.9652	100	18271.1	100	60.0229	100	7064.84	100	0.0876327
η	10.6385	76.18	9292.88	50.86	42.1034	70.15	5383.75	76.2	0.0876893
p^T	3.21582	30.23	3646.03	39.23	25.8532	61.4	1194.66	22.19	0.0460979
ΔR	2.61978	81.47	3174.62	87.07	21.8961	84.69	0	0	0.0463369
$\lvert M_{jj} - M_W\rvert < 20\,\text{GeV}$	2.57127	98.15	379.156	11.94	3.19114	14.57	0	100	0.131498
$\lvert M_{l^+l^-} - M_Z\rvert > 20\,\text{GeV}$	0.873261	33.96	11.0076	2.903	1.80668	56.62	0	100	0.243948
$\lvert M^T_{\text{vis}} - m_{H_2}\rvert < 50\,\text{GeV}$	0.797024	91.27	2.00562	18.22	0.274929	15.22	0	100	0.527778
$\lvert M_{\text{all}} - m_{H_2}\rvert < 50\,\text{GeV}$	0.741578	84.92	1.16606	10.59	0.147283	8.152	0	100	0.647095

	BP2($ee\mu$)	Eff. %	$WZjj$	Eff. %	$t\bar{t}l\nu$	Eff. %	$t\bar{t}$	Eff. %	$S/\sqrt{B}$
No cuts.	15.4415	100	19574.3	100	185.155	100	21486.4	100	0.0760323
η	12.0316	77.92	9957.39	50.87	130.277	70.36	16520.9	76.89	0.0737585
p^T	3.68017	30.59	3652.42	36.68	76.7151	58.89	3164.68	19.16	0.0443239
ΔR	3.22968	87.76	3177.7	87	65.0109	84.74	0	0	0.056716
$\lvert M_{jj} - M_W\rvert < 20\,\text{GeV}$	3.19503	98.93	377.85	11.89	8.31661	12.79	0	100	0.162588
$\lvert M_{l^+l^-} - M_Z\rvert > 20\,\text{GeV}$	2.28711	71.58	21.3155	5.641	6.79468	81.7	0	100	0.431375
$\lvert M^T_{\text{vis}} - m_{H_2}\rvert < 50\,\text{GeV}$	2.07226	90.61	4.10453	19.26	1.4532	21.39	0	100	0.879015
$\lvert M_{\text{all}} - m_{H_2}\rvert < 50\,\text{GeV}$	1.8782	82.12	2.51869	11.82	0.638228	9.393	0	100	1.05709

Table 4. Benchmark point BP2. Luminosity $\mathcal{L} = 100\,\text{fb}^{-1}$. Universal acceptance cuts = $|\eta_l| < 2.5$, $|\eta_j| < 3$, $p^T_{j_{1,2}} > 30\,\text{GeV}$, $\Delta R_{jj} > 0.4 + \Delta R_{lj} > 0.4 + \Delta R_{ll} > 0.3$. Transverse momentum cuts for the eee category: $p^T_{e_{1,2}} > 28\,\text{GeV}$ and $p^T_{e_3} > 5\,\text{GeV}$. Transverse momentum cuts for the $ee\mu$ category: $p^T_{e_{1,2}} > 14\,\text{GeV}$ and $p^T_{\mu} > 10\,\text{GeV}$.

	BP2($e\mu\mu$)	Eff. %	$WZjj$	Eff. %	$t\bar{t}l\nu$	Eff. %	$t\bar{t}$	Eff. %	$S/\sqrt{B}$
No cuts.	15.8573	100	19613.8	100	187.639	100	21109.9	100	0.0783984
η	12.1841	76.84	10031.1	51.14	132.82	70.78	16298.2	77.21	0.0748997
p^T	3.99205	32.76	3776.77	37.65	81.6147	61.45	3599.54	22.09	0.046226
ΔR	3.35443	84.03	3287.72	87.05	69.8418	85.58	0	0	0.0578904
$\lvert M_{jj} - M_W\rvert < 20\,\text{GeV}$	3.28512	97.93	394.687	12	9.82872	14.07	0	100	0.163337
$\lvert M_{l^+l^-} - M_Z\rvert > 20\,\text{GeV}$	2.48117	75.53	25.6999	6.511	8.02204	81.62	0	100	0.427268
$\lvert M^T_{\text{vis}} - m_{H_2}\rvert < 50\,\text{GeV}$	2.3079	93.02	6.11015	23.77	1.48265	18.48	0	100	0.837561
$\lvert M_{\text{all}} - m_{H_2}\rvert < 50\,\text{GeV}$	2.06533	83.24	4.24445	16.52	0.864063	10.77	0	100	0.913781

	BP2($\mu\mu\mu$)	Eff. %	$WZjj$	Eff. %	$t\bar{t}l\nu$	Eff. %	$t\bar{t}$	Eff. %	$S/\sqrt{B}$
No cuts.	14.3326	100	18102	100	64.9422	100	6901.4	100	0.0905235
η	11.0266	76.93	9214.47	50.9	45.9328	70.73	5336.08	77.32	0.0912682
p^T	4.33858	39.35	3910.77	42.44	32.4907	70.74	1428.14	26.76	0.0591975
ΔR	3.6871	84.98	3401.86	86.99	27.7482	85.4	0	0	0.0629597
$\lvert M_{jj} - M_W\rvert < 20\,\text{GeV}$	3.62472	98.31	413.624	12.16	3.85883	13.91	0	100	0.177401
$\lvert M_{l^+l^-} - M_Z\rvert > 20\,\text{GeV}$	1.54553	42.64	15.252	3.687	2.16016	55.98	0	100	0.370383
$\lvert M^T_{\text{vis}} - m_{H_2}\rvert < 50\,\text{GeV}$	1.35147	87.44	3.21832	21.1	0.422213	19.55	0	100	0.708313
$\lvert M_{\text{all}} - m_{H_2}\rvert < 50\,\text{GeV}$	1.18514	76.68	2.19219	14.37	0.186559	8.636	0	100	0.768414

Table 5. Benchmark point BP2. Luminosity $\mathcal{L} = 100\,\text{fb}^{-1}$. Universal acceptance cuts = $|\eta_l| < 2.5$, $|\eta_j| < 3$, $p^T_{j_{1,2}} > 30\,\text{GeV}$, $\Delta R_{jj} > 0.4 + \Delta R_{lj} > 0.4 + \Delta R_{ll} > 0.3$. Transverse momentum cuts for the eee category: $p^T_{e_{1,2}} > 35\,\text{GeV}$ and $p^T_{e_3} > 5\,\text{GeV}$. Transverse momentum cuts for the $ee\mu$ category: $p^T_{e_{1,2}} > 14\,\text{GeV}$ and $p^T_\mu > 10\,\text{GeV}$.

	BP1	Eff. %	$WZjj$	Eff. %	$t\bar{t}l\nu$	Eff. %	$t\bar{t}$	Eff. %	$S/\sqrt{B}$
No cuts.	11.4362	100	242279	100	1505.03	100	294324	100	0.01559
η	10.5155	91.95	124514	51.39	1062.12	70.57	224375	76.23	0.019332
p^T	6.87307	65.36	1073.8	0.8624	5.39058	0.5075	93.3936	0.04162	0.307085
ΔR cuts	1.39939	20.36	628.972	58.57	3.26969	60.66	0	0	0.273344
$\Delta R_{jj} < 1.5$	1.27106	90.83	178.267	28.34	0.412394	12.61	0	100	0.104689
$\lvert M_{jj} - M_W \rvert < 20\,\text{GeV}$	1.24427	97.89	35.8213	20.09	0.117827	28.57	0	100	0.212022
$\lvert M_{l^+l^-} - M_Z \rvert > 20\,\text{GeV}$	1.14049	91.66	0.699635	1.953	0.117827	100	0	100	1.3762
$\lvert M^T_{\text{vis}} - M_{Z'} \rvert < 1\,\text{TeV}$	0.950781	83.37	0	0	0	0	0	100	-

	BP2	Eff. %	$WZjj$	Eff. %	$t\bar{t}l\nu$	Eff. %	$t\bar{t}$	Eff. %	$S/\sqrt{B}$
No cuts.	7.62627	100	242279	100	1505.03	100	294324	100	0.0103963
η	7.04229	92.34	124514	51.39	1062.12	70.57	224375	76.23	0.0128916
p^T	5.04656	71.66	1073.8	0.8624	5.39058	0.5075	93.3936	0.04162	0.205656
ΔR cuts	1.33571	26.47	628.972	58.57	3.26969	60.66	0	0	0.200703
$\Delta R_{jj} < 1.5$	1.30044	97.36	178.267	28.34	0.412394	12.61	0	100	0.0999255
$\lvert M_{jj} - M_W \rvert < 20\,\text{GeV}$	1.27536	98.07	35.8213	20.09	0.117827	28.57	0	100	0.216923
$\lvert M_{l^+l^-} - M_Z \rvert > 20\,\text{GeV}$	1.18835	93.18	0.699635	1.953	0.117827	100	0	100	1.41058
$\lvert M^T_{\text{vis}} - M_{Z'} \rvert < 1\,\text{TeV}$	1.10055	92.61	0	0	0	0	0	100	inf

Table 6. Benchmark point BP1 for the Z'-mediator case. Luminosity $\mathcal{L} = 300\,\text{fb}^{-1}$. Universal acceptance cuts = $|\eta_l| < 2.5$, $|\eta_j| < 3$, $p^T_{j_{1,2}} > 30\,\text{GeV}$, ΔR cuts = $\Delta R_{jj} > 0.4 + \Delta R_{lj} > 0.4 + \Delta R_{ll} > 0.3$. Transverse momentum cuts: $p^T_{l_1} > 300\,\text{GeV}$, $p^T_{l_2} > 150\,\text{GeV}$ and $p^T_{l_3} > 15\,\text{GeV}$.

	BP1	Eff. %	$WZjj$	Eff. %	$t\bar{t}l\nu$	Eff. %	$t\bar{t}$	Eff. %	WZj	Eff. %
Fat Jet(100)	10.1885	89.09	113051	46.66	765.197	50.84	99452.5	27.38	47731	24.8
Fat Jet(130)	9.70868	84.89	85950.7	35.48	467.007	31.03	48839	13.45	33767.8	17.55
Fat Jet(150)	9.46763	82.79	71715.2	29.6	328.855	21.85	31891	8.781	27100.2	14.08
Fat Jet(170)	9.29913	81.31	59914.6	24.73	231.353	15.37	22300.6	6.14	21814.6	11.34
Fat Jet(200)	9.05139	79.15	45985.6	18.98	136.296	9.056	14429.3	3.973	15986	8.307

	BP2	Eff. %	$WZjj$	Eff. %	$t\bar{t}l\nu$	Eff. %	$t\bar{t}$	Eff. %	WZj	Eff. %
Fat Jet(100)	7.12303	93.4	113051	46.66	765.197	50.84	99452.5	27.38	47731	24.8
Fat Jet(130)	6.86827	90.06	85950.7	35.48	467.007	31.03	48839	13.45	33767.8	17.55
Fat Jet(150)	6.73266	88.28	71715.2	29.6	328.855	21.85	31891	8.781	27100.2	14.08
Fat Jet(170)	6.58529	86.35	59914.6	24.73	231.353	15.37	22300.6	6.14	21814.6	11.34
Fat Jet(200)	6.42773	84.28	45985.6	18.98	136.296	9.056	14429.3	3.973	15986	8.307

Table 7. BP1 and BP2 benchmark points for the Z'-mediator case. Luminosity $\mathcal{L} = 300\,\text{fb}^{-1}$. Fat jet definition (first column) and efficiencies for signal and SM background as explained in the text. The minimum p^T in GeV required for the fat jet is given in parenthesis. The efficiencies are not cumulative.

	BP1	Eff. %	$WZjj$	Eff. %	$t\bar{t}l\nu$	Eff. %	$t\bar{t}$	Eff. %	WZj	Eff. %	$S/\sqrt{B}$
No cuts.	11.4362	100	242279	100	1505.03	100	363181	100	192436	100	0.0122192
Fat Jet(200)	9.05139	79.15	45985.6	18.98	136.296	9.056	14429.3	3.973	15986	8.307	0.0413375
$p_j^T/p_J^T < 0.25$	9.04804	99.96	31324.6	68.12	43.7137	32.07	8974.54	62.2	15986	100	0.0381373
$\lvert\eta_l\rvert < 2.5$	8.60278	95.08	24281	77.51	38.0875	87.13	7964.72	88.75	12118.1	75.8	0.0429392
$p_{l_i}^T > 300, 150, 15\,\text{GeV}$	6.74028	78.35	1046.65	4.311	1.14881	3.016	70.0452	0.8794	392.486	3.239	0.221362
$1l$ inside Fat Jet	5.54734	82.3	131.252	12.54	0.972071	84.62	64.2081	91.67	57.307	14.6	0.42314
$\Delta R_{ll} > 0.3$	4.92353	88.75	95.85	73.03	0.913158	93.94	55.4524	86.36	43.9798	76.74	0.396041
$p_l^{T,rel} > 200\,\text{GeV}$	4.0888	83.05	3.91796	4.088	0.0294567	3.226	0	0	1.33272	3.03	2.14266
$\lvert M_{l^+l^-} - M_Z\rvert > 20\,\text{GeV}$	3.75737	91.89	0.139927	3.571	0.0294567	100	0	100	0	0	9.93483

	BP2	Eff. %	$WZjj$	Eff. %	$t\bar{t}l\nu$	Eff. %	$t\bar{t}$	Eff. %	WZj	Eff. %	$S/\sqrt{B}$
No cuts.	7.62627	100	242279	100	1505.03	100	363181	100	192436	100	0.00852962
Fat Jet(200)	6.42773	84.28	45985.6	18.98	136.296	9.056	14429.3	3.973	15986	8.307	0.0275661
$p_j^T/p_J^T < 0.25$	6.42773	100	31324.6	68.12	43.7137	32.07	8974.54	62.2	15986	100	0.0270827
$\lvert\eta_l\rvert < 2.5$	6.00288	93.39	24281	77.51	38.0875	87.13	7964.72	88.75	12118.1	75.8	0.030504
$p_{l_i}^T > 300, 150, 15\,\text{GeV}$	5.07399	84.53	1046.65	4.311	1.14881	3.016	70.0452	0.8794	392.486	3.239	0.154462
$\Delta R_{lJ} > 0.8$	4.93289	97.22	891.195	85.15	0.117827	10.26	0	0	325.184	82.85	0.145477
$\Delta R_{ll} > 0.3$	4.58564	92.96	637.927	71.58	0.117827	100	0	100	262.879	80.84	0.164345
$p_l^{T,rel} > 400\,\text{GeV}$	3.36829	73.45	76.5401	12	0	0	0	100	31.3189	11.91	0.441542
$\lvert M_{l^+l^-} - M_Z\rvert > 20\,\text{GeV}$	3.17075	94.14	1.25934	1.645	0	100	0	100	0.99954	3.191	2.24111

Table 8. BP1 and BP2 benchmark points for the Z'-mediator case. Luminosity $\mathcal{L} = 300\,\text{fb}^{-1}$. Cut flow and efficiencies for signal and SM background as explained in the text.

JHEP02(2018)109

References

[1] P. Langacker, *Grand Unified Theories and Proton Decay*, *Phys. Rept.* **72** (1981) 185 [INSPIRE].

[2] J.L. Hewett and T.G. Rizzo, *Low-Energy Phenomenology of Superstring Inspired E_6 Models*, *Phys. Rept.* **183** (1989) 193 [INSPIRE].

[3] A.E. Faraggi and D.V. Nanopoulos, *A superstring Z' at O(1-TeV)?*, *Mod. Phys. Lett.* **A 6** (1991) 61 [INSPIRE].

[4] A.E. Faraggi and M. Guzzi, *Extra Z' s and W' s in heterotic-string derived models*, *Eur. Phys. J.* **C 75** (2015) 537 [arXiv:1507.07406] [INSPIRE].

[5] A.E. Faraggi and J. Rizos, *The 750 GeV di-photon LHC excess and extra Z's in heterotic-string derived models*, *Eur. Phys. J.* **C 76** (2016) 170 [arXiv:1601.03604] [INSPIRE].

[6] L. Randall and R. Sundrum, *A Large mass hierarchy from a small extra dimension*, *Phys. Rev. Lett.* **83** (1999) 3370 [hep-ph/9905221] [INSPIRE].

[7] E. Accomando, A. Belyaev, L. Fedeli, S.F. King and C. Shepherd-Themistocleous, *Z' physics with early LHC data*, *Phys. Rev.* **D 83** (2011) 075012 [arXiv:1010.6058] [INSPIRE].

[8] S. Khalil and A. Masiero, *Radiative B-L symmetry breaking in supersymmetric models*, *Phys. Lett.* **B 665** (2008) 374 [arXiv:0710.3525] [INSPIRE].

[9] L. Basso, A. Belyaev, S. Moretti and C.H. Shepherd-Themistocleous, *Phenomenology of the minimal B-L extension of the Standard model: Z' and neutrinos*, *Phys. Rev.* **D 80** (2009) 055030 [arXiv:0812.4313] [INSPIRE].

[10] L. Basso, S. Moretti and G.M. Pruna, *Constraining the g_1' coupling in the minimal $B-L$ Model*, *J. Phys.* **G 39** (2012) 025004 [arXiv:1009.4164] [INSPIRE].

[11] L. Basso, A. Belyaev, S. Moretti, G.M. Pruna and C.H. Shepherd-Themistocleous, *Z' discovery potential at the LHC in the minimal $B-L$ extension of the Standard Model*, *Eur. Phys. J.* **C 71** (2011) 1613 [arXiv:1002.3586] [INSPIRE].

[12] L. Basso, S. Moretti and G.M. Pruna, *Phenomenology of the minimal $B-L$ extension of the Standard Model: the Higgs sector*, *Phys. Rev.* **D 83** (2011) 055014 [arXiv:1011.2612] [INSPIRE].

[13] L. Basso, S. Moretti and G.M. Pruna, *A Renormalisation Group Equation Study of the Scalar Sector of the Minimal B-L Extension of the Standard Model*, *Phys. Rev.* **D 82** (2010) 055018 [arXiv:1004.3039] [INSPIRE].

[14] L. Basso, S. Moretti and G.M. Pruna, *Theoretical constraints on the couplings of non-exotic minimal Z' bosons*, *JHEP* **08** (2011) 122 [arXiv:1106.4762] [INSPIRE].

[15] L. Basso, K. Mimasu and S. Moretti, *Z' signals in polarised top-antitop final states*, *JHEP* **09** (2012) 024 [arXiv:1203.2542] [INSPIRE].

[16] L. Basso, K. Mimasu and S. Moretti, *Non-exotic Z' signals in $\ell^+\ell^-$, $b\bar{b}$ and $t\bar{t}$ final states at the LHC*, *JHEP* **11** (2012) 060 [arXiv:1208.0019] [INSPIRE].

JHEP02(2018)109

[17] E. Accomando, D. Becciolini, A. Belyaev, S. Moretti and C. Shepherd-Themistocleous, *Z' at the LHC: Interference and Finite Width Effects in Drell-Yan*, *JHEP* **10** (2013) 153 [arXiv:1304.6700] [INSPIRE].

[18] E. Accomando, A. Belyaev, J. Fiaschi, K. Mimasu, S. Moretti and C. Shepherd-Themistocleous, *Forward-backward asymmetry as a discovery tool for Z' bosons at the LHC*, *JHEP* **01** (2016) 127 [arXiv:1503.02672] [INSPIRE].

[19] E. Accomando, A. Belyaev, J. Fiaschi, K. Mimasu, S. Moretti and C. Shepherd-Themistocleous, *A_{FB} as a discovery tool for Z' bosons at the LHC*, *Nuovo Cim.* **C 38** (2016) 153 [arXiv:1504.03168] [INSPIRE].

[20] N. Okada and S. Okada, *Z'_{BL} portal dark matter and LHC Run-2 results*, *Phys. Rev.* **D 93** (2016) 075003 [arXiv:1601.07526] [INSPIRE].

[21] N. Okada and S. Okada, *Z'-portal right-handed neutrino dark matter in the minimal $\mathrm{U}(1)_X$ extended Standard Model*, *Phys. Rev.* **D 95** (2017) 035025 [arXiv:1611.02672] [INSPIRE].

[22] G. Brooijmans et al., *Les Houches 2011: Physics at TeV Colliders New Physics Working Group Report*, arXiv:1203.1488 [INSPIRE].

[23] A. Caputo, P. Hernández, J. Lopez-Pavon and J. Salvado, *The seesaw portal in testable models of neutrino masses*, *JHEP* **06** (2017) 112 [arXiv:1704.08721] [INSPIRE].

[24] A.M. Gago, P. Hernández, J. Jones-Pérez, M. Losada and A. Moreno Briceño, *Probing the Type I Seesaw Mechanism with Displaced Vertices at the LHC*, *Eur. Phys. J.* **C 75** (2015) 470 [arXiv:1505.05880] [INSPIRE].

[25] P.S. Bhupal Dev, R. Franceschini and R.N. Mohapatra, *Bounds on TeV Seesaw Models from LHC Higgs Data*, *Phys. Rev.* **D 86** (2012) 093010 [arXiv:1207.2756] [INSPIRE].

[26] C.G. Cely, A. Ibarra, E. Molinaro and S.T. Petcov, *Higgs Decays in the Low Scale Type I See-Saw Model*, *Phys. Lett.* **B 718** (2013) 957 [arXiv:1208.3654] [INSPIRE].

[27] I.M. Shoemaker, K. Petraki and A. Kusenko, *Collider signatures of sterile neutrinos in models with a gauge-singlet Higgs*, *JHEP* **09** (2010) 060 [arXiv:1006.5458] [INSPIRE].

[28] S. Antusch, E. Cazzato and O. Fischer, *Displaced vertex searches for sterile neutrinos at future lepton colliders*, *JHEP* **12** (2016) 007 [arXiv:1604.02420] [INSPIRE].

[29] S. Antusch, E. Cazzato and O. Fischer, *Sterile neutrino searches at future e^-e^+, pp and e^-p colliders*, *Int. J. Mod. Phys.* **A 32** (2017) 1750078 [arXiv:1612.02728] [INSPIRE].

[30] S. Antusch, E. Cazzato and O. Fischer, *Sterile neutrino searches via displaced vertices at LHCb*, *Phys. Lett.* **B 774** (2017) 114 [arXiv:1706.05990] [INSPIRE].

[31] A. Das, *Pair production of heavy neutrinos in next-to-leading order QCD at the hadron colliders in the inverse seesaw framework*, arXiv:1701.04946 [INSPIRE].

[32] A. Das and N. Okada, *Bounds on heavy Majorana neutrinos in type-I seesaw and implications for collider searches*, *Phys. Lett.* **B 774** (2017) 32 [arXiv:1702.04668] [INSPIRE].

[33] A. Das, P.S.B. Dev and C.S. Kim, *Constraining Sterile Neutrinos from Precision Higgs Data*, *Phys. Rev.* **D 95** (2017) 115013 [arXiv:1704.00880] [INSPIRE].

[34] E. Accomando, L. Delle Rose, S. Moretti, E. Olaiya and C.H. Shepherd-Themistocleous, *Novel SM-like Higgs decay into displaced heavy neutrino pairs in $\mathrm{U}(1)'$ models*, *JHEP* **04** (2017) 081 [arXiv:1612.05977] [INSPIRE].

JHEP02(2018)109

[35] Z. Kang, P. Ko and J. Li, *New Avenues to Heavy Right-handed Neutrinos with Pair Production at Hadronic Colliders*, *Phys. Rev.* **D 93** (2016) 075037 [arXiv:1512.08373] [INSPIRE].

[36] M. Mitra, R. Ruiz, D.J. Scott and M. Spannowsky, *Neutrino Jets from High-Mass W_R Gauge Bosons in TeV-Scale Left-Right Symmetric Models*, *Phys. Rev.* **D 94** (2016) 095016 [arXiv:1607.03504] [INSPIRE].

[37] O. Mattelaer, M. Mitra and R. Ruiz, *Automated Neutrino Jet and Top Jet Predictions at Next-to-Leading-Order with Parton Shower Matching in Effective Left-Right Symmetric Models*, arXiv:1610.08985 [INSPIRE].

[38] E. Accomando, C. Corianò, L. Delle Rose, J. Fiaschi, C. Marzo and S. Moretti, *Search for Z', vacuum (in)stability and hints of high-energy structures*, *EPJ Web Conf.* **129** (2016) 00007 [arXiv:1609.05652] [INSPIRE].

[39] E. Accomando, C. Corianò, L. Delle Rose, J. Fiaschi, C. Marzo and S. Moretti, *Phenomenology of minimal Z' models: from the LHC to the GUT scale*, *EPJ Web Conf.* **129** (2016) 00006 [arXiv:1609.05029] [INSPIRE].

[40] E. Accomando, C. Corianò, L. Delle Rose, J. Fiaschi, C. Marzo and S. Moretti, *Z', Higgses and heavy neutrinos in $\mathrm{U}(1)'$ models: from the LHC to the GUT scale*, *JHEP* **07** (2016) 086 [arXiv:1605.02910] [INSPIRE].

[41] C. Corianò, L. Delle Rose and C. Marzo, *Constraints on abelian extensions of the Standard Model from two-loop vacuum stability and $\mathrm{U}(1)_{B-L}$*, *JHEP* **02** (2016) 135 [arXiv:1510.02379] [INSPIRE].

[42] P. Langacker, *The Physics of Heavy Z' Gauge Bosons*, *Rev. Mod. Phys.* **81** (2009) 1199 [arXiv:0801.1345] [INSPIRE].

[43] J. Erler, P. Langacker, S. Munir and E. Rojas, *Improved Constraints on Z' Bosons from Electroweak Precision Data*, *JHEP* **08** (2009) 017 [arXiv:0906.2435] [INSPIRE].

[44] G. Cacciapaglia, C. Csáki, G. Marandella and A. Strumia, *The Minimal Set of Electroweak Precision Parameters*, *Phys. Rev.* **D 74** (2006) 033011 [hep-ph/0604111] [INSPIRE].

[45] E. Salvioni, G. Villadoro and F. Zwirner, *Minimal Z' models: Present bounds and early LHC reach*, *JHEP* **11** (2009) 068 [arXiv:0909.1320] [INSPIRE].

[46] CMS collaboration, *Search for narrow resonances in dilepton mass spectra in proton-proton collisions at $\sqrt{s} = 13$ TeV and combination with 8 TeV data*, *Phys. Lett.* **B 768** (2017) 57 [arXiv:1609.05391] [INSPIRE].

[47] P. Bechtle, O. Brein, S. Heinemeyer, G. Weiglein and K.E. Williams, *HiggsBounds: Confronting Arbitrary Higgs Sectors with Exclusion Bounds from LEP and the Tevatron*, *Comput. Phys. Commun.* **181** (2010) 138 [arXiv:0811.4169] [INSPIRE].

[48] P. Bechtle, O. Brein, S. Heinemeyer, G. Weiglein and K.E. Williams, *HiggsBounds 2.0.0: Confronting Neutral and Charged Higgs Sector Predictions with Exclusion Bounds from LEP and the Tevatron*, *Comput. Phys. Commun.* **182** (2011) 2605 [arXiv:1102.1898] [INSPIRE].

[49] P. Bechtle et al., *Recent Developments in HiggsBounds and a Preview of HiggsSignals*, PoS(CHARGED2012)024 [arXiv:1301.2345] [INSPIRE].

[50] P. Bechtle et al., HiggsBounds – 4*: Improved Tests of Extended Higgs Sectors against Exclusion Bounds from LEP, the Tevatron and the LHC*, *Eur. Phys. J.* **C 74** (2014) 2693 [arXiv:1311.0055] [INSPIRE].

JHEP02(2018)109

[51] P. Bechtle, S. Heinemeyer, O. Stal, T. Stefaniak and G. Weiglein, *Applying Exclusion Likelihoods from LHC Searches to Extended Higgs Sectors*, *Eur. Phys. J.* **C 75** (2015) 421 [arXiv:1507.06706] [INSPIRE].

[52] P. Bechtle, S. Heinemeyer, O. Stal, T. Stefaniak and G. Weiglein, *HiggsSignals: Confronting arbitrary Higgs sectors with measurements at the Tevatron and the LHC*, *Eur. Phys. J.* **C 74** (2014) 2711 [arXiv:1305.1933] [INSPIRE].

[53] A. Belyaev, N.D. Christensen and A. Pukhov, *CalcHEP 3.4 for collider physics within and beyond the Standard Model*, *Comput. Phys. Commun.* **184** (2013) 1729 [arXiv:1207.6082] [INSPIRE].

[54] G. Brooijmans et al., *Les Houches 2011: Physics at TeV Colliders New Physics Working Group Report*, arXiv:1203.1488 [INSPIRE].

[55] CMS collaboration, *Search for* $\mathrm{t\bar{t}}$ *resonances in highly boosted lepton+jets and fully hadronic final states in proton-proton collisions at* $\sqrt{s} = 13$ *TeV*, *JHEP* **07** (2017) 001 [arXiv:1704.03366] [INSPIRE].

[56] F. Gianotti et al., *Physics potential and experimental challenges of the LHC luminosity upgrade*, *Eur. Phys. J.* **C 39** (2005) 293 [hep-ph/0204087] [INSPIRE].

JHEP02(2018)109